

NOVEL APPROACHES FOR PREPARATION OF NANOPARTICLES

1

Bolla G. Rao, Deboshree Mukherjee, Benjaram M. Reddy*CSIR-Indian Institute of Chemical Technology, Hyderabad, India*

CHAPTER OUTLINE

1	Introduction.....	1
1.1	Evolution of Metal Nanoparticles in Pharmacy and Biotechnology.....	2
2	Synthetic Methods for Preparation of Metal Nanoparticles	5
2.1	Thermal Decomposition Method	5
2.2	Sol-Gel Method	8
2.3	Hydrothermal and Solvothermal Method.....	10
2.4	Microwave-Assisted Method	13
2.5	Polyol Method	15
2.6	Sonochemical Method.....	17
2.7	Liquid–Liquid Interface Method	17
2.8	Phase-Transfer Method.....	21
2.9	Biosynthesis Method	22
2.10	Template-Directed Synthetic Method	24
3	Application of Metal Nanoparticles in Theranostics	27
3.1	Diagnosis and Drug Delivery.....	27
4	Conclusions.....	31
	References.....	31

1 INTRODUCTION

Since the beginning of the 21st century, with the rising concern of multidrug resistance and scarcity of new antibiotics, the use of metal nanoparticles (NPs) in medicine is undergoing renaissance. In contrast to bulk, nanomaterials exhibit huge surface area per unit volume and tunable optical, electronic, magnetic, and biological properties. Metal NPs can be engineered to have different sizes, shapes, and surface characteristics. The size and shape tunable properties of metal nanoparticles and their wide scope of applicability in pharmacy and biotechnology have drawn global attention toward their size and shape-controlled synthesis. However, while dealing with metal nanoparticle synthesis, few things should be considered seriously. First, the chosen method must be simple, less expensive, ecofriendly,

and commercially viable. Second, the simultaneous control of particle size and shape along with their uniformity is another key objective (Kwon and Hyeon, 2008). Moreover, the NPs are kinetically unstable, they should be stabilized against aggregation into larger particles (Richter et al., 2010). Micelles, polymers, and coordinative ligands are frequently used as stabilizers to control the growth of NPs (Kim et al., 2004). Solution-based nanofabrication methods usually offer more control and reproducibility over the metal NPs. A wide range of nanofabrication methods, including precipitation, deposition-precipitation, sol-gel, liquid-liquid interface technique, hydrothermal and solvothermal syntheses, microwave-assisted processes, polyol method, template-directed synthesis, ionic-liquid assisted methods, and so on are reported in the literature. In this chapter, the frequently used fabrication techniques are addressed in detail with appropriate literature references. A careful study of their usefulness and drawbacks with special importance on the laboratory scale synthesis has also been discussed with appropriate illustrations.

1.1 EVOLUTION OF METAL NANOPARTICLES IN PHARMACY AND BIOTECHNOLOGY

Medicinal application of metals is already known from the ancient time. The Ebers Papyrus from 1500 BC is the earliest written account of the use of metals for treatment and describes more than 800 recipes. It has mentioned the use of copper to reduce inflammation and the use of iron to treat anemia. Sushruta Samhita, the ancient book on Indian Ayurvedic treatment methodology written around 7th century BC, mentioned the use of some primary metals like gold, silver, copper, lead, tin, zinc, and iron in medicines (Prakash, 1997). Sodium vanadate has also been used since the early 20th century to treat rheumatoid arthritis. Antimicrobial properties of metals are also known, and have been in use for thousands of years. For example, copper and silver vessels have been used for water disinfection and food preservation since the time of the Persian kings. This practice was later adopted by the Phoenicians, Greeks, Romans, and Egyptians (Alexander, 2009). Settlers of North America used to drop Ag coins into transport containers to preserve water, wine, milk, and vinegar, and a similar strategy was used by Japanese soldiers during the Second World War to prevent the spread of dysentery (Borkow and Gabbay, 2009). The medicinal use of metals was prevalent until the discovery of antibiotics by Nobel laureate Sir Alexander Fleming in the 1920s.

Reducing the metal particle size to nanorange (<100 nm), however, has been demonstrated as an efficient and reliable tool for improving biocompatibility (Taton et al., 2000). Earlier studies have shown that antimicrobial formulations in the form of NPs could be used as effective bactericidal materials (Fresta et al., 1995). Later on, it was revealed that highly reactive metal oxide NPs exhibit excellent biocidal action against Gram-positive and Gram-negative bacteria (Stoimenov et al., 2002). Zero-valent metal nanoparticles like, Au, Ag, and FeNPs, as well as, metal oxide NPs like, zinc oxide (ZnO), titanium dioxide (TiO₂), magnesium oxide (MgO), etc., exhibit bactericidal activity and have been found to be stable and safe for human beings (Lemire et al., 2013). The intrinsic properties and related possible applications of different metal NPs are mainly dependent on their size, shape, composition, crystallinity, and morphology (Dickson and Lyon, 2000). NP toxicity may arise from several attributes, which include the traits that are specific to the properties of the NPs, such as size, shape, or surface charge, and traits that control the release of metal ions (El Badawy et al., 2011; Morones et al., 2005; Pal et al., 2007). The toxic mode of action of NPs has also been connected with the generation of reactive oxygen species (ROS) and membrane disruption (Fig. 1.1) (Bandyopadhyay et al., 2012; Gunawan et al., 2011). A striking capability that has been reported for many NPs is their

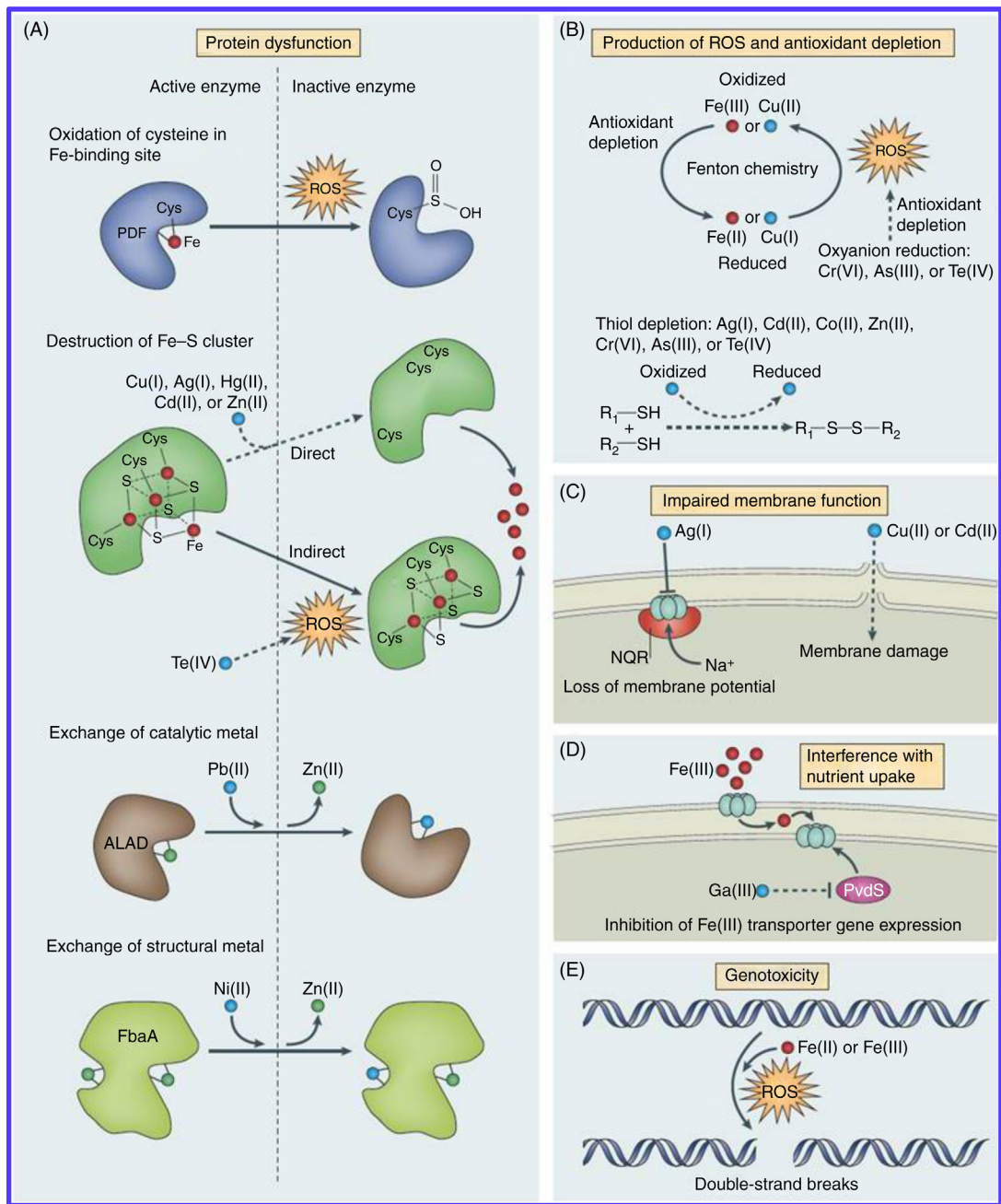


FIGURE 1.1 Antibacterial Mechanisms of Metal Toxicity

(A) Metals can lead to protein dysfunction. (B) Production of reactive oxygen species (ROS) and depletion of antioxidants. (C) Certain metals have been shown to impair membrane function. (D) Interference with nutrient assimilation. (E) They can also be genotoxic. *Solid arrows* represent elucidated biochemical mechanism, whereas, *dashed arrows* represent a route of toxicity for which the underlying biochemical mechanism is unclear. *ALAD*, δ-Aminolevulinic acid dehydratase; *FbaA*, fructose-1,6-bisphosphate aldolase; *NQR*, NADH; quinone oxidoreductase; *PDF*, peptide deformylase; *PvdS*, a σ-factor (σ24) from *Pseudomonas aeruginosa*.

Reprinted with permission from Lemire, J.A., Harrison, J.J., Raymond, J., 2013. Antimicrobial activity of metals: mechanisms, molecular targets and applications. *Nat. Rev. Microbiol.* 11, 371–384. Copyright 2013, Macmillan Publishers Limited.

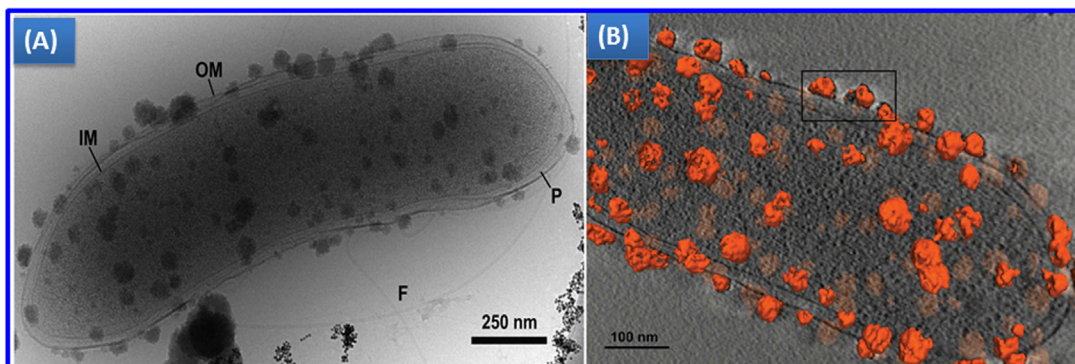


FIGURE 1.2

(A) The figure shows cryo-TEM image of a single cell planktonic Fe-reducing bacterium isolated from groundwater at a site in Rifle, Colorado, USA. (B) A 3-D construction of nanoaggregates [orange (mid-gray in print version)] attached to the groundwater bacterium cell wall (Luef et al., 2013).

Reprinted with permission from Bao, Y., An, W., Turner, C.W., Krishnan, K.M., 2010. The critical role of surfactants in the growth of cobalt nanoparticles. Langmuir 26, 478–483. Copyright 2013, International Society for Microbial Ecology.

ability to physically interact with the cell surfaces of some bacteria. For example, Fe-reducing bacteria that naturally accumulate NPs of ferric oxyhydroxide at their cell surface (Fig. 1.2) can be exploited in targeting a specific bacterial cell (Luef et al., 2013). However, a large number of reports in the literature indicate that the driving force behind the antimicrobial properties of antibacterial NPs is the release of ions (Xiu et al., 2012). Tactically designed NPs, which release ions in a controlled manner or can be targeted to specific bacterial cells, have numerous antimicrobial applications and bagged a business of US\$17.5 billion in the year 2011 in global market (Lemire et al., 2013).

Metal and metal oxide NPs have also found applications in advanced techniques of therapeutics, diagnosis, and drug delivery. For example, there are a wide range of paramagnetic metal NPs, mostly but not exclusively based on iron; when an external magnetic field is applied, these NPs become magnetic themselves, and align themselves with the direction of the external field, showing up as a hypoexposed region on an MRI scan (Edmundson et al., 2003). Iron-based magnetic NPs, such as Feridex, have mostly been used in in vitro or in vivo experiments, for example, in tracking the movement of stem cells implanted into a wound site (Okada et al., 2005). In recent times, nanometer-sized crystals made of metallic or semiconductor materials, known as quantum dots have gained much popularity in synthetic biology (Nath and Banerjee, 2013).

Shape-dependent optical activity of the metal NPs has brought a revolution in the field of bioimaging and diagnosis. Huang and coworkers demonstrated that due to longitudinal absorption band in the near infrared (NIR), Au-nanorods are effective in acoustic imaging and are suitable as photothermal agents for hyperthermia therapy of cancer cells. Small diameter Au-nanorods are being used as photothermal converters of near infrared radiation (NIR) for in vivo applications due to their high absorption cross-sections beyond the tissue absorption spectra (Huang et al., 2006a,b). Gold nanocages and nanoframes developed by Xia and coworkers also exhibit potential biomedical applications due to their desirable optical properties and cargo-holding hollow structures (Skrabalak et al., 2008). Silica-gold

core–shell NPs, or gold nanoshells, have attracted much attention due to their interesting optical properties and numerous biomedical applications. Aden and Kerker (1951) predicted that concentric spherical particles could exhibit tunable plasmon resonance which vary as a function of the ratio of shell thickness to core radius. Other gold nanostructures, such as Au-nanoshells, Au-nanocages, and spherical AuNPs have also demonstrated effective photothermal destruction of cancer cells and tissue (Conde et al., 2011). Novel optical properties of other related structures, such as asymmetric “nanoeggs” and quadruply concentric “nanomtryushkas” have also been explored (Wang et al., 2007).

2 SYNTHETIC METHODS FOR PREPARATION OF METAL NANOPARTICLES

2.1 THERMAL DECOMPOSITION METHOD

Thermal decomposition method is an excellent synthetic route to fabricate metal NPs. This method is facile and involves single step process. It is inexpensive, environmentally benign, and provides higher quality of metal NPs in terms of morphology, size, and particle-size distribution (Luo et al., 2009). It is a well-known fact from literature that, nucleation step and particle growth are the crucial factors to achieve monodisperse NPs (Kashchiev and van Rosmalen, 2003). The size and shape of the NP can be tuned in thermal decomposition method by controlling the previously mentioned factors by the use of appropriate surfactants. This method involves thermal decomposition of organometallic precursor, like metal carbonyls and metal surfactant complex in solution resulting in metallic NPs (Kwon and Hyeon, 2008). For example, Bao et al. (2010) have synthesized monodisperse cobalt NPs using $\text{CO}_2(\text{CO})_8$ as the precursor and oleic acid (OA), tri-*n*-octylphosphine oxide (TOPO), and di-*n*-octylamine (DOA) as the surfactants. Fig. 1.3 shows the TEM images of CoNPs at different time periods in the presence of OA and TOPO surfactants. The particle size was found to rapidly increase with respect to time period. Growth pathway was also investigated in terms of the influence of the surfactant. Combination of OA and TOPO provides diffusional growth pathway, whereas OA and DOA combination and TOPO alone allowed aggregation and ripening growth pathways, respectively. In a similar way, metallic Cu and PdNPs were prepared using precursors, copper cupferronate $\text{Cu}(\text{cupf})_2$ complex, and Pd-trioctylphosphine complex, respectively in the presence of trioctylphosphine (TOP) and DOA surfactant. The concentration of stabilizing or capping agent (TOP) played a vital role in controlling the particle size (Diab et al., 2011; Kim et al., 2003).

Chen et al. (2007) have reported the preparation of monodisperse spherical NiNPs via thermal decomposition of nickel (II) acetylacetone (Ni (acac)₂) complex in the presence of various alkyl amines. Reaction temperature and solvent type exhibit profound influence on the crystalline phase of NiNPs, whereas, surfactants played a significant role in controlling the particle size as well as morphology. Kura et al. (2010) successfully synthesized monodisperse FeNPs with high saturation magnetization from $\text{Fe}(\text{CO})_x\text{-OAm}$ precursor, in which CO ligands are partially replaced with OAm. During the course of the reaction the precursor decomposed and yielded monodispersed FeNPs. However, OAm played a significant role as a ligand and surfactant to produce small Fe particles by covering the surface of the metal particle.

Kim et al. (2007) have reported the synthesis of hollow iron nanoframes by thermal decomposition of Fe (II)–oleate complex, yielding uniform size Fe nanocubes in the presence of oleic acid. Fig. 1.4 shows various morphologies of iron and inset shows the HRTEM image of FeNPs. However, the addition of a little amount of sodium oleate to the reaction solution, resulted in a remarkable change in the

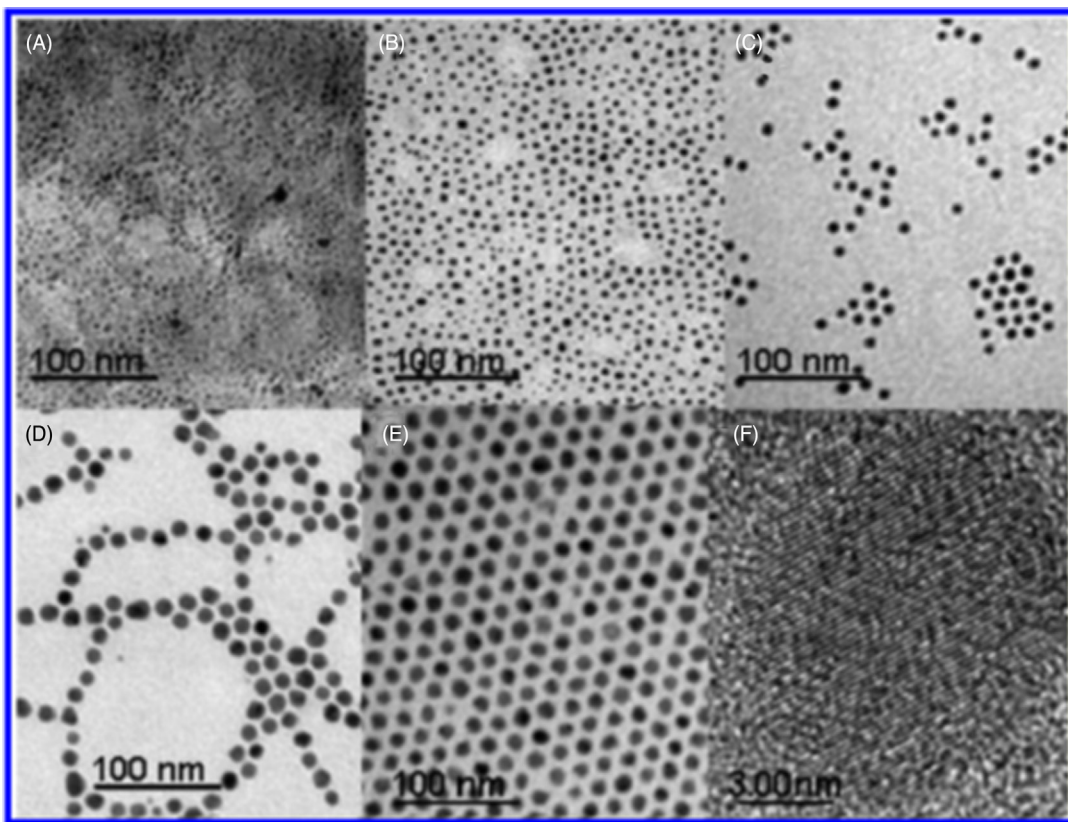


FIGURE 1.3 TEM Images of Co Nanoparticles (NPs) in the Presence of Surfactants OA and TOPO at Different Stages

(A) 1, (B) 5, (C) 10, (D) 15, and (E) 30 min. (F) High resolution of TEM image of Co NPs.

Reprinted with permission from Bao, Y., An, W., Turner, C.W., Krishnan, K.M., 2010. The critical role of surfactants in the growth of cobalt nanoparticles. *Langmuir* 26, 478–483. Copyright 2010, American Chemical Society.

morphology of FeNPs, that is, nanocubes to nanoframes. Therefore, it is believed that sodium oleate played a significant role in controlling the morphology of the Fe NPs and the obtained Fe nanoframes showed exceptional biomedical applications, especially in drug delivery. A wide variety of bimetallic NPs have also been prepared by thermal decomposition method (Samia et al., 2006). For instance, Cu–Pt bimetallic NPs with 1.2-nm size were synthesized by thermolysis of corresponding metal precursors— $\text{Pt}(\text{acac})_2$ and $\text{Cu}(\text{acac})_2$ at 498 K under oleylamine (Zheng et al., 2003). EXAFS studies revealed that, Pt atoms occupied the Cu sites. Charge transfer from Cu to Pt was observed during the formation of Cu–Pt bimetallic system. Kang and Murray (2010) have reported the synthesis of Mn–Pt bimetallic nanocubes using $[\text{Mn}(\text{acac})_2]$ or $\text{Mn}_2(\text{CO})_{10}$ with platinum acetylacetone $[\text{Pt}(\text{acac})_2]$ in the presence of oleylamine and oleic acid stabilizers.

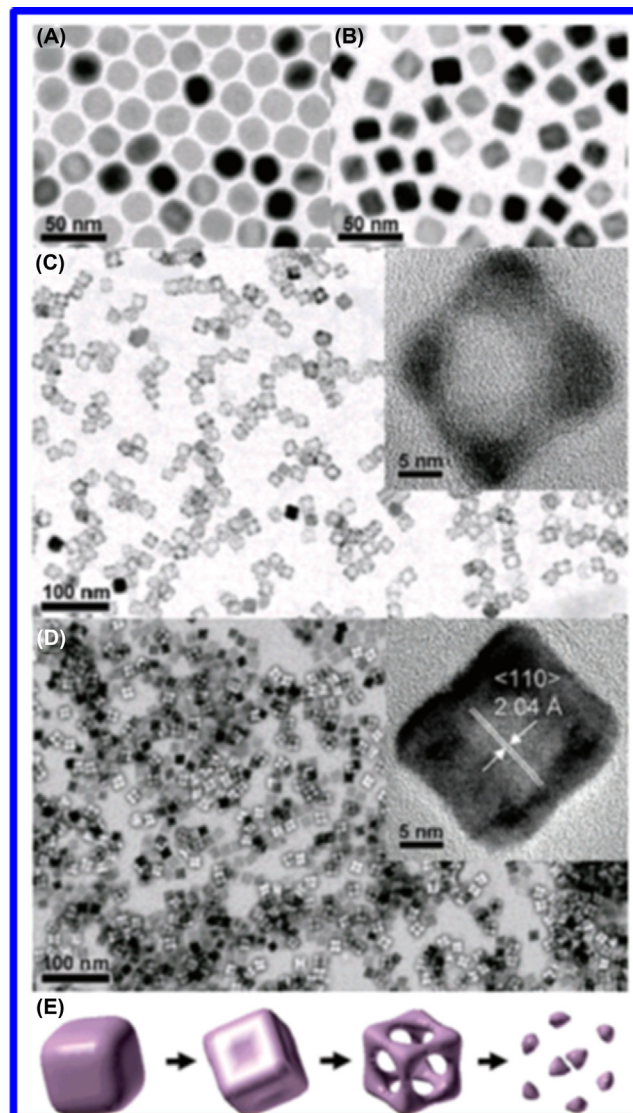


FIGURE 1.4 TEM Images of FeNPs

(A) 23-nm sized spheres with slightly faceted shape, (B) 21-nm sized nanocubes, (C) 21-nm sized nanoframes (inset HRTEM), (D) 17-nm sized particles with intermediate shape between *solid* and *hollow* nanocubes (inset HRTEM), (E) the overall shape evolution of the Fe nanoparticles.

Reprinted with permission from Kim, D., Park, J., An, K., Yang, N.K., Park, J.G., Hyeon, T., 2007. Synthesis of hollow iron nanoframes. J. Am. Chem. Soc. 129, 5812–5813. Copyright 2007, American Chemical Society.

2.2 SOL-GEL METHOD

Sol-gel method is one of the well-established synthetic approaches to prepare novel metal oxide NPs as well as mixed oxide composites. This method has potential control over the textural and surface properties of the materials. Sol-gel method mainly undergoes in few steps to deliver the final metal oxide protocols and those are hydrolysis, condensation, and drying process. The formation of metal oxide involves different consecutive steps, initially the corresponding metal precursor undergoes rapid hydrolysis to produce the metal hydroxide solution, followed by immediate condensation which leads to the formation of three-dimensional gels. Afterward, obtained gel is subjected to drying process, and the resulting product is readily converted to Xerogel or Aerogel based on the mode of drying. Sol-gel method can be classified into two routes, such as aqueous sol-gel and nonaqueous sol-gel method depending on the nature of the solvent utilized.

If water is used as reaction medium it is known as aqueous sol-gel method; and use of organic solvent as reaction medium for sol-gel process is termed as nonaqueous sol-gel route. The reaction pathway for the production of metal oxide nanostructures in the sol-gel method is shown in Fig. 1.5. In the sol-gel approach, nature of metal precursor and solvent plays a remarkable role in the synthesis of metal oxides NPs.

2.2.1 Aqueous sol-gel method

In aqueous sol-gel method, oxygen is necessary for the formation of metal oxide, which is supplied by the water solvent. Generally, metal acetates, nitrates, sulfates, chlorides, and metal alkoxides are employed as the metal precursors for this method. However, metal alkoxides are widely used as the

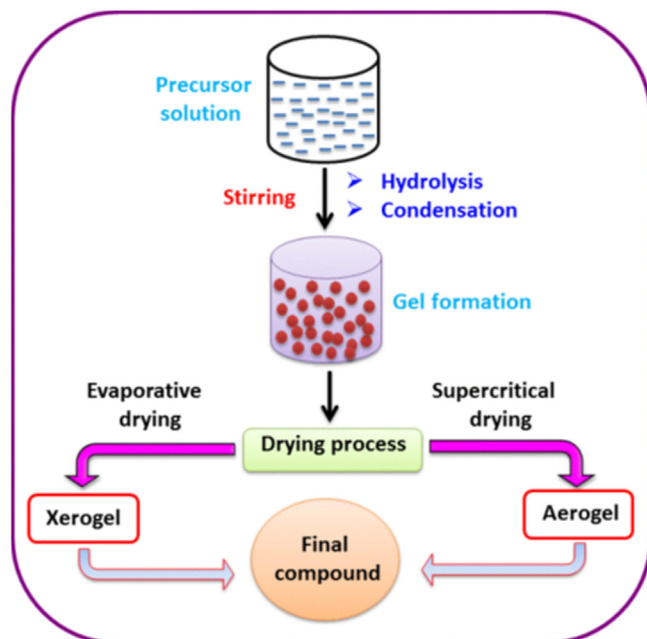


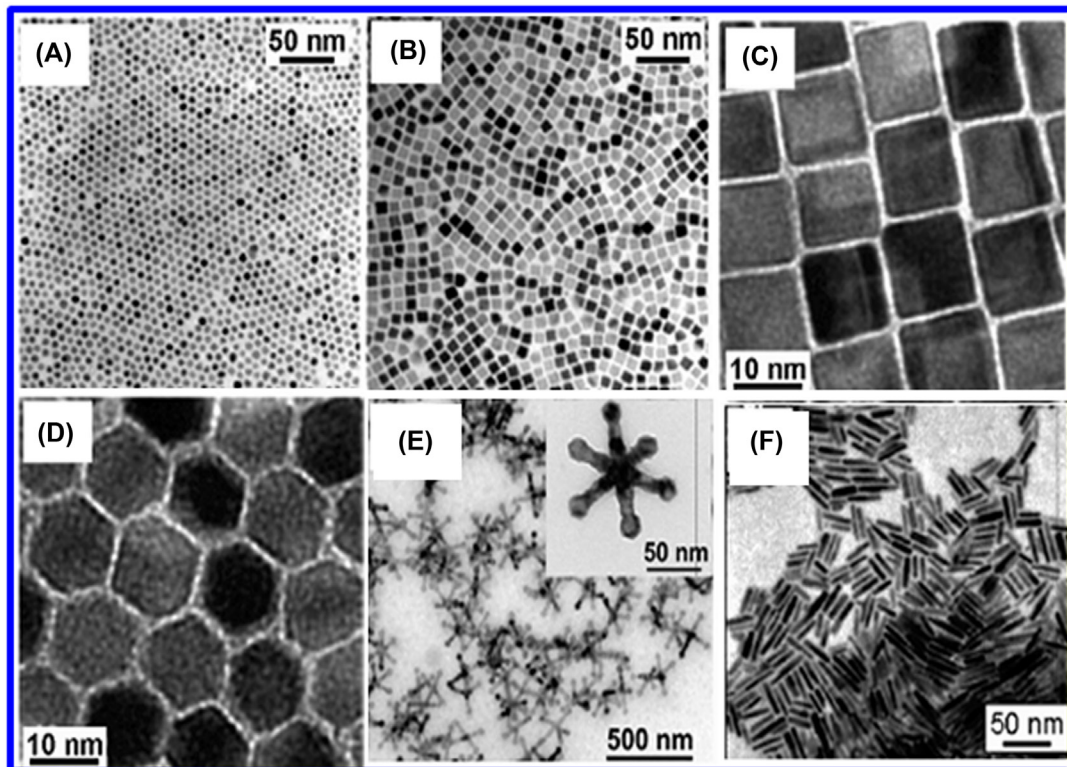
FIGURE 1.5 The Reaction Pathway for the Production of Metal Oxide Nanostructures in the Sol-Gel Method

precursors for the production of metal oxide NPs, due to high reaction affinity of alkoxides toward water (Bradley et al., 2001; Turova and Turevskaya, 2002). However, some difficulties are associated with the aqueous sol–gel method. The key steps, such as hydrolysis, condensation, and drying take place simultaneously in a number of cases resulting in difficulty in controlling particle morphology, and reproducibility of the final protocol during the sol–gel process (Corriu and Leclercq, 1996). The aforementioned difficulties, however, do not affect much of the synthesis of metal oxides in bulk, but strongly affect the preparation of nanooxides. Therefore, it is believed that the aqueous sol–gel route is highly recommended for the synthesis of bulk metal oxides rather than their nanoscale counterparts (Niederberger, 2007).

2.2.2 Nonaqueous sol–gel method

Nonaqueous or nonhydrolytic sol–gel method is devoid of some of the major drawbacks found in aqueous sol–gel method. In nonaqueous sol–gel process, oxygen required for the formation of metal oxide is supplied from the solvents, such as alcohols, ketones, aldehydes, or by the metal precursors. Furthermore, these organic solvents not only serve as oxygen providers but also offer a versatile tool for tuning several key components like morphology, surface properties, particle size, and composition of the final oxide material. Although, nonaqueous sol–gel approach is not as popular as aqueous sol–gel method; nonaqueous sol–gel routes have shown excellent impact on the production of nanooxides compared to that of aqueous sol–gel route. The nonaqueous sol–gel route can be divided into two important methodologies, namely, surfactant-controlled and solvent-controlled approaches for the production of metal oxide NPs. Surfactant-controlled strategy involves direct transformation of metal precursor into the respective metal oxide at higher temperature range in hot injection method. This method permits outstanding control over the shape, growth of the NP, and avoids the agglomeration of particles. Few examples of surfactant-controlled synthesized NPs are mentioned here for understanding. Song and Zhang (2004) have demonstrated the simple nonhydrolytic route to synthesize high-quality spherical-shaped CoFe_2O_4 NPs with 8-nm size. However, the spherical morphology can be changed to cubic shape with 10-nm edge length during the seed-mediated growth. Heating rate and growth temperature played a pivotal role in controlling the shape of CoFe_2O_4 nanomaterial (Fig. 1.6A–B).

The resulting materials were subjected to shape-dependent magnetic properties. Zeng et al. (2004) have extensively studied the shape-controlled synthesis of MnFe_2O_4 nanomaterial. The relative ratio between surfactant and $\text{Fe}(\text{acac})_3$ showed a remarkable role in controlling the final morphology of MnFe_2O_4 . TEM analysis revealed the formation of cube-like or polyhedron-type morphology for MnFe_2O_4 (Fig. 1.6C–D). In addition, size of MnFe_2O_4 particle is dependent on the concentration of metal precursors. Novel cone-shaped ZnO was obtained by decomposition of TOPO– $\text{Zn}(\text{OAc})_2$ complex resulting in the formation of hierarchically ordered spheres of cone-shaped ZnO nanocrystals (Joo et al., 2005). Li et al. (2006) fabricated titanium oxide nanorods with 3.3-nm diameter and a length of 25 nm using appropriate amounts of reaction ingredients, such as titanium butoxide, triethylamine, linoleic acid, and cyclohexane. Reaction temperature, time, and concentration of the reactant were found to show huge effect on the shape and size of the TiONPs. Preparation of high-quality single crystalline MnO multipods with homogeneous size and shape, involved decomposition of $\text{Mn}(\text{oleate})_2$ in the presence of oleic acid and *n*-trioctylamine (Fig. 1.6E) (Zitoun et al., 2005). Tungsten oxide nanorods were generated by treatment of WCl_4 with oleylamine and oleic acid (Fig. 1.6F) (Seo et al., 2005). Solvent-controlled sol–gel route, involves the reaction between metal halide and alcohols to produce metal oxide nanostructures. For example, porous SnO_2 NPs were prepared by the addition of tin chloride to benzylalcohol under stirring condition, which was immediately dispersed in THF solution, producing

**FIGURE 1.6**

TEM images of (A) 8-nm sized spherical CoFe_2O_4 NPs and (B) cube-like CoFe_2O_4 NPs. TEM images of (C) cube-like and (D) polyhedron-shaped MnFe_2O_4 NPs. (E) TEM image of MnO multipods (inset, hexapod). (F) TEM image of Tungsten oxide nanorods.

Part (A–B): Reproduced from Song, Q., Zhang, Z.J., 2004. Shape control and associated magnetic properties of spinel cobalt ferrite nanocrystals. J. Am. Chem. Soc. 126, 6164–6168. Copyright 2004, American Chemical Society. Part (C–D): Reprinted from Zeng, H., Rice, P.M., Wang, S.X., Sun, S.H., 2004. Shape-controlled synthesis and shape-induced texture of MnFe_2O_4 nanoparticles. J. Am. Chem. Soc. 126, 11458–11459. Copyright 2004, American Chemical Society. Part (E): Reproduced from Zitoun, D., Pinna, N., Frolet, N., Belin, C., 2005. Single crystal manganese oxide multipods by oriented attachment. J. Am. Chem. Soc. 127, 15034–15035. Copyright 2005, American Chemical Society. Part (F): Reproduced from Seo, J.-W., Jun, Y.-W., Ko, S.J., Cheon, J., 2005. In situ one-pot synthesis of 1-dimensional transition metal oxide nanocrystals. J. Phys. Chem. B. 109, 5389–5391. Copyright 2005, American Chemical Society.

sol. The subsequent addition of block polymer to sol allowed mesoporous nanostructure for SnO_2 by the elimination of solvent molecule ([Ba et al., 2005](#)).

2.3 HYDROTHERMAL AND SOLVOTHERMAL METHOD

Hydrothermal or solvothermal method is one of the most common and effective synthetic routes to fabricate the nanomaterial with a variety of morphologies. In this method, the reactants are placed into

an autoclave filled with water or organic compound to carry out the reaction under high temperature and pressure conditions. If the nonaqueous solvents are utilized as reaction medium, it is termed as solvothermal method; whereas, in case the preparation is carried out in the presence of water, it is known as hydrothermal process (Cushing et al., 2004; Wu et al., 2002). Different kinds of autoclaves and their functions are deeply discussed in the literature (Hakuta et al., 2005; Rabenau, 1985). Generally, Teflon-lined autoclaves are capable of working at high temperature and pressure. In addition, it sustains alkaline media and exhibits a strong resistance to hydrofluoric acid when compared to glass and quartz autoclaves. Therefore, Teflon-lined autoclave is chosen as an ideal container to perform the reaction under desired conditions. Precise control in hydrothermal process is the key factor that enables the synthesis of various nanostructured inorganic materials (Shi et al., 2013). This method can facilitate and accelerate the reaction among the reactants, promote hydrolysis, followed by crystal growth resulting in self-assembly of nanomaterials in the solution. Moreover, the properties, morphology, size, and structure of nanomaterials can be tailored easily by varying the different reaction parameters, such as reaction time, temperature, reaction medium, pressure, pH, and concentration of the reactants and filled volume of autoclave. This method can be suitable for the preparation of nanomaterials with a variety of shapes as compared to other methodologies.

Yan et al. (2008) have fabricated ceria nanoctahedrons and nanorods without assistance of surfactant or template via simple and facile hydrothermal approach. High quality of ceria nanorods with 20-nm width and few hundred nanometer length were produced by treating $\text{Ce}(\text{NO}_3)_3 \cdot 6\text{H}_2\text{O}$ with $\text{Na}_3\text{PO}_4 \cdot 6\text{H}_2\text{O}$ in water medium (Fig. 1.7A). The change in the morphology of the ceria NPs was achieved by tuning the hydrothermal reaction time. It was demonstrated that, Na_3PO_4 played a crucial role in the formation of

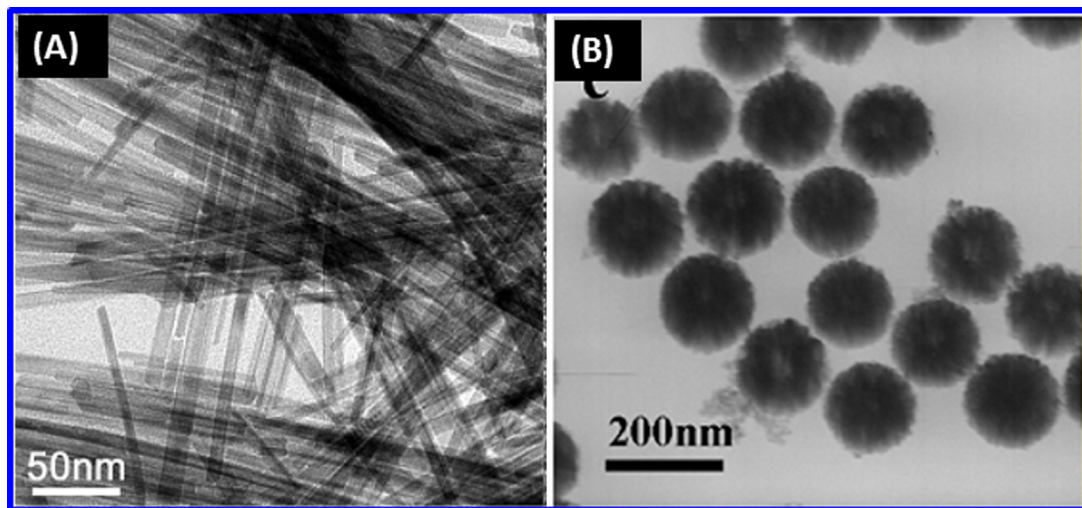


FIGURE 1.7 TEM image of (A) CeO_2 nanorod. (B) TEM image of CeO_2 hollow sphere.

Part (A): Reprinted with permission from Yan, L., Yu, R., Chen, J., Xing, X., 2008. Template-free hydrothermal synthesis of CeO_2 nanoctahedrons and nanorods: investigation of the morphology evolution. *Cryst. Growth Des.* 8, 1474–1477. Copyright 2008, American Chemical Society. Part (B): Reprinted with permission from Yang, Z., Han, D., Ma, D., Liang, H., Liu, L., Yang, Y., 2010. Fabrication of monodisperse CeO_2 hollow spheres assembled by nanoctahedra, *Cryst. Growth Des.*, 10, 291–295. Copyright 2010, American Chemical Society.

ceria nanostructures. A simple hydrothermal method has been developed to prepare ceria nanocubes and octahedra by employing $\text{Ce}(\text{NO}_3)_3 \cdot 6\text{H}_2\text{O}$, $\text{Na}_3\text{PO}_4 \cdot 6\text{H}_2\text{O}$, and NaOH as precursors. The obtained nanostructured ceria was effectively studied for CO oxidation reaction. Interestingly, after the exposure of these nanoshapes to CO oxidation at 673 K, they have retained their original shape without losing their individual nanoshape, indicating that these nanostructures are thermally stable up to 673 K (Zili et al., 2012).

Yang et al. (2010) have demonstrated that nanoctahedra are the building blocks for the production of monodisperse ceria hollow spheres that are obtained by mild hydrothermal route (Fig. 1.7B). H_2O_2 played a significant role in the production of novel hollow sphere nanostructures, whereas polyvinylpyrrolidone (PVP) played an important role in promoting the nucleation of nanocrystals during the course of reaction. The alignment of hollow sphere nanostructure of ceria was explained based on the Ostwald ripening mechanism. Van et al. (2012) have reported the synthesis of Fe_2O_3 nanostructure with a variety of morphologies by using capping agents like sodium carboxymethyl cellulose (CMC) and hydrazine (N_2H_4) assisted hydrothermal method (Fig. 1.8). Capping agents can produce different morphologies, such as spheres and truncated hexagonal pyramid-shaped Fe_2O_3 nanocrystals. However, without the aid of capping agent dendrite shape of Fe_2O_3 nanocrystals were obtained. Therefore, it is believed that capping agents play a vital role in controlling the morphology of final nanomaterial. Magnetic and optical properties of nanostructured hematite phase Fe_2O_3 nanocrystals were extensively studied.

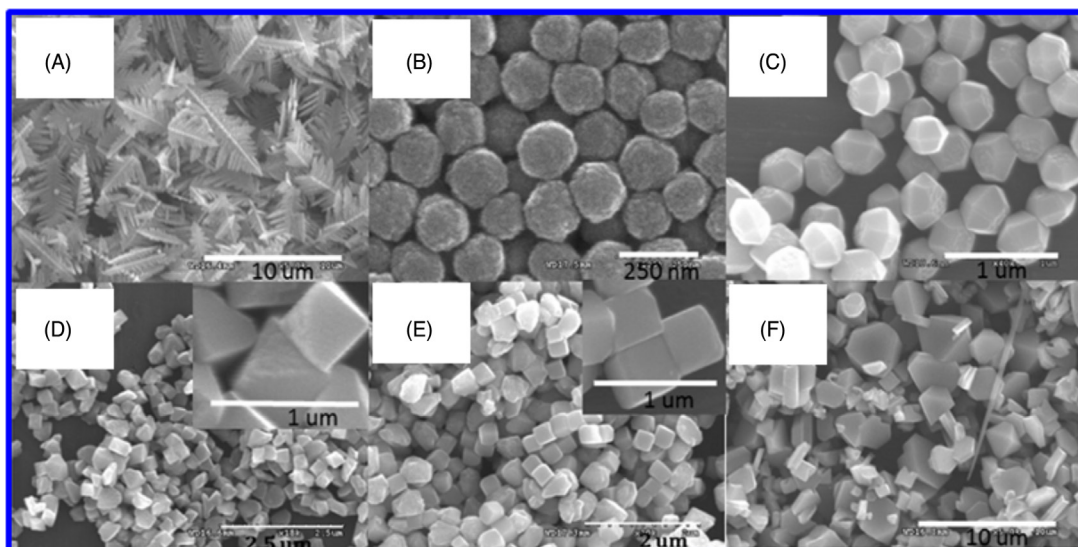


FIGURE 1.8 Morphology of $\alpha\text{-Fe}_2\text{O}_3$ With Various Reactants Under Hydrothermal Conditions at 433 K for 8 h

(A) $\text{K}_3[\text{Fe}(\text{CN})_6]$, 0.02 M, in the absence of CMC and N_2H_4 ; (B) $\text{K}_3[\text{Fe}(\text{CN})_6]$, in the absence of CMC, 3.5 gL^{-1} ; (C) $\text{K}_3[\text{Fe}(\text{CN})_6]$, 0.02 M, with the addition of CMC, 3.5 gL^{-1} and N_2H_4 , 1.5 wt.%; (D) $\text{K}_3[\text{Fe}(\text{CN})_6]$, 0.02 M, with the addition of CMC, 3.5 gL^{-1} , and N_2H_4 , 4.5 wt.%; (E) $\text{K}_3[\text{Fe}(\text{CN})_6]$, 0.02 M, with the addition of CMC, 3.5 gL^{-1} , and N_2H_4 , 6.0 wt.%; (F) $\text{K}_3[\text{Fe}(\text{CN})_6]$, 0.02 M, with the addition of CMC, 3.5 gL^{-1} , and N_2H_4 , 8.0 wt.%.

Reprinted with permission from Van, T.-K., Cha, H.G., Nguyen, C.K., Kim, S.-W., Jung, M.-H., Kang, Y.S., 2012. Nanocrystals of hematite with unconventional shape-truncated hexagonal bipyramid and its optical and magnetic properties. *Cryst. Growth Des.* 12, 862–868. Copyright 2011, American Chemical Society.

2.4 MICROWAVE-ASSISTED METHOD

Generally, solution-based approaches utilize conventional heating, which is the driving force for chemical reactions. In this process, heat energy is transferred from the source to the solvent and then transferred to reactants during the course of the reaction. However, conventional heating process inevitably suffers from various drawbacks, including high thermal gradient effects, slow reaction kinetics, nonconsistent and undesirable reaction conditions throughout the bulk (Gerbec et al., 2005). Particularly, for large-scale production of NPs, the aforesaid problematic aspects, such as inhomogeneity, poor crystallization, and thermal gradient effects may be magnified tremendously resulting in poor nucleation and wide-size distribution (Hu et al., 2008; Hu and Yu, 2008). From this point of view, microwave method is one of the excellent alternative routes to address the previously mentioned issues raised in conventional heating process.

Microwaves are nothing but electromagnetic energy with frequency in the range of 300 MHz to 300 GHz. Generally, interaction of microwaves with materials during the reaction is based on two important mechanisms: dipole interactions and ionic conduction. However, these two mechanisms can effectively work, when coupling takes place between components of target compound and oscillating electric field of microwave. Fig. 1.9 depicts the production of heat energy during the interaction of microwaves with polar water molecule (Tsuji et al., 2005). In microwave frequency range, water molecules try to orient with the electric field and the two polar ends try to reorient with respect to the oscillating electric field, as a result they lose energy in the form of heat by molecular collision and friction. Other polar molecules, such as alcohols, DMF, ethylene glycol are used as ideal solvents for microwave-assisted synthesis of metal NPs, due to their high dielectric loss and high reduction ability.

Microwave method received considerable attention as a new, promising, and environmental friendly method to synthesize the metallic nanostructures as well as metal oxides with a variety of morphologies. In addition, microwave strategy offers several benefits, such as high efficiency in the utilization of heat. Moreover, it is clean, cheap, and produces higher yields of desired materials within shorter reaction times. Fast and uniform heating of reaction mixture throughout the solution are the beneficial factors. These factors always allow the rapid decomposition of respective metal precursors followed by the nucleation and subsequent growth to obtain the required nanostructures (Gerbec et al., 2005). A wide variety of metal NPs and metal oxide NP with control over size and morphology of the NPs to tailor their properties have been synthesized by adopting the microwave-assisted method.

Mohamed et al. (2010) have explored various morphologies, such as spherical, truncated prisms, and hexagons for AuNP by using HAuCl₄ in HCl as gold precursor via microwave-assisted strategy

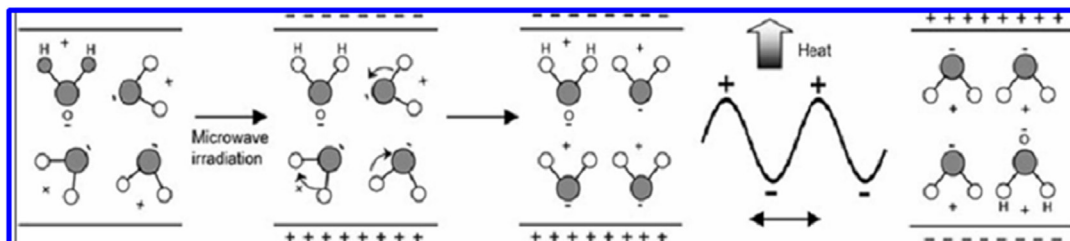
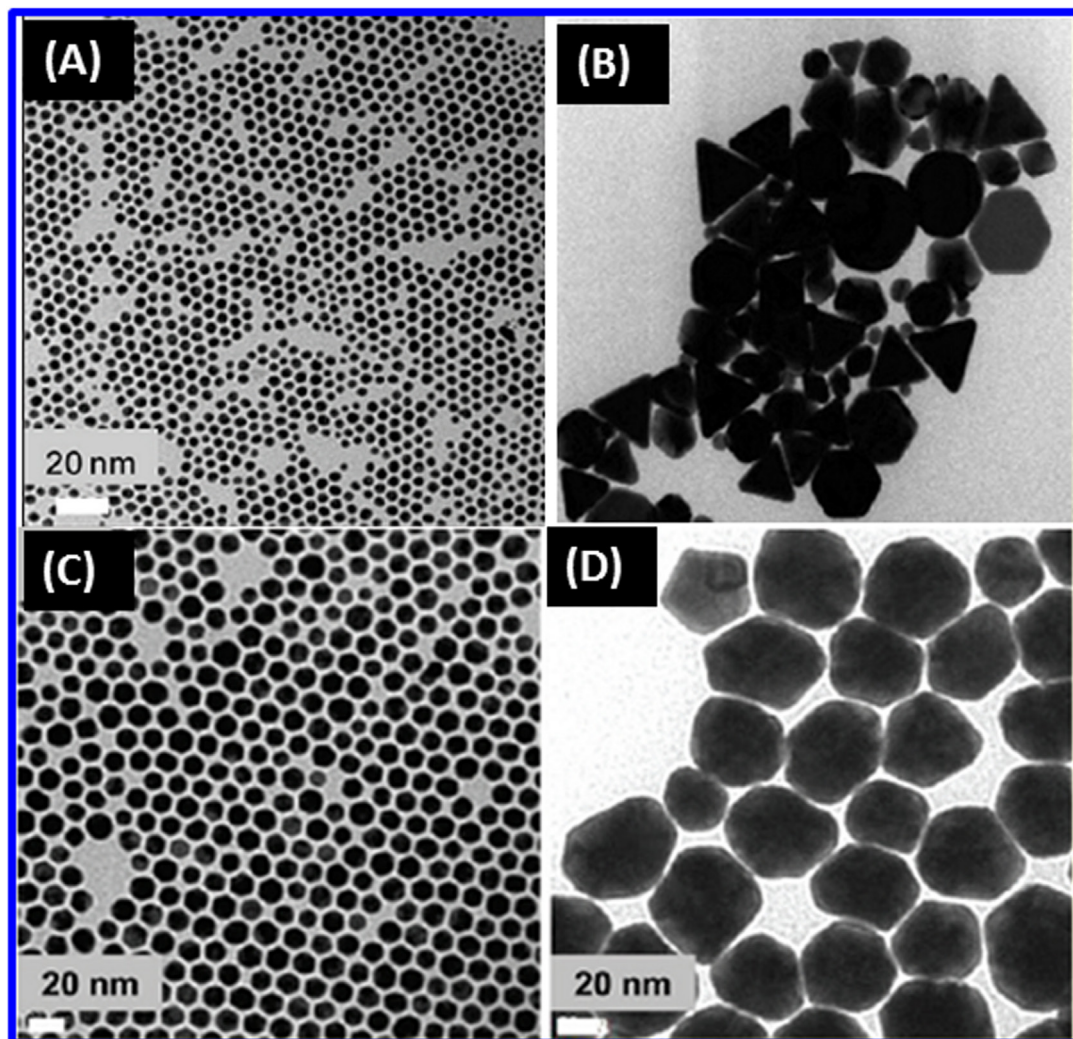


FIGURE 1.9 Production of Heat Energy by Microwave Irradiation of Water Molecule

Reprinted with permission from Tsuji, M., Hashimoto, M., Nishizawa, Y., Kubokawa, M., Tsuji, T., 2005. *Microwave-assisted synthesis of metallic nanostructures in solution*. *Chem. Eur. J.* 11, 440–452. Copyright 2005, Wiley-VCH.

**FIGURE 1.10**

TEM image of (A) AuNPs prepared using pure amine, (B) AuNPs prepared in 70% oleic acid, (C–D) AuNPs formed using 9 and 36 mM of HAuCl₄, respectively.

Reprinted with permission from Mohamed, M.B., AbouZeid, K.M., Abdelsayed, V., Aljarash, A.A., Samy El-Shall, M., 2010. Growth mechanism of anisotropic gold nanocrystals via microwave synthesis: formation of dioleamide by gold nanocatalysis. ACS Nano 4, 2766–2772. Copyright 2010, American Chemical Society.

(Fig. 1.10). Oleylamine and oleic acid mixture served as capping agents to control the particle size. The oleic acid and oleylamine ratio, concentration of gold precursor and microwave exposure time profoundly influence the size and morphology of Au nanocrystals. Also, these factors show a favorable role in tuning the surface resonance properties of the resulting nanocrystals in visible and near-infrared regions. [Mallikarjuna and Varma \(2007\)](#) have successfully generated various nanostructures of noble metal NPs, such as gold, silver, platinum, and palladium in bulk quantities, with particle size in the range of 2–15 nm, by reduction of respective metal salts using D-glucose, maltose, and sucrose solutions via microwave-assisted method. The type of reducing sugar was found to be a vital parameter in determining the morphology of the resultant nanomaterial. As prepared noble metal NPs showed versatile applications in various fields including catalysis, biosensors, energy storage systems, and nanodevices.

Microwave-assisted strategy offers precise control over the various key parameters, such as morphology, crystallinity, nucleation, and growth of the monodisperse Pd, Pt, and RhNPs compared to conventional heating method. Recently, our group prepared different ceria-based mixed oxides, such as $\text{CeO}_2\text{-ZrO}_2$, $\text{CeO}_2\text{-SiO}_2$, and $\text{CeO}_2\text{-Al}_2\text{O}_3$ and others by microwave-induced combustion process. In this method, stoichiometric ratios of corresponding metal nitrate precursors were added to the desired quantity of urea. The resulting mixtures were heated in a microwave oven for 40 min; as a result, mixed oxides were generated. The metal mixed oxides prepared by MW showed high oxygen vacancies and lattice defects compared to the coprecipitation method ([Reddy et al., 2009a,b,c, 2010](#)).

2.5 POLYOL METHOD

A number of promising synthetic routes have been employed to synthesize different kinds of NPs with a variety of morphologies. Among them, polyol method is a versatile liquid-phase method utilizing high boiling and multivalent alcohols to produce the NPs. Polyols played a dual role as a reducing agent and solvent, also they are capable of controlling the particle growth. The polyol synthetic route was first introduced in 1989 by Fievets group where they used the term polyol for metal NPs synthesis. Several kinds of polyols that include, ethylene glycol (EG), propylene glycol (PG), butylene glycol (BG), diethylene glycol (DG), triethylene glycol (TrEG), tetraethylene glycol (TEG), and so on up to polyethylene glycol (PEG) have been utilized in this process ([Carroll et al., 2011](#); [Grisaru et al., 2003](#)). However, the polyols provide excellent advantages in terms of various aspects. The high boiling point of polyols can allow the synthesis in the temperature range of 473–593 K without high pressure and autoclave. The good capabilities of polyols to solubilize the starting materials allow the use of simple and cheap metal precursors as starting compounds. The chelating ability of polyol is a beneficial factor to control key features, such as nucleation, growth, and agglomeration of the particles. Another important advantage of polyols is that the reductive ability at elevated temperatures can reduce the metal solution readily to form metal NPs. The selection of polyol for the preparation of NPs is highly dependent on two aspects, those are boiling point and reduction potential of the polyol.

[Wang et al. \(2013\)](#) developed a robust polyol method for preparation of Ag nanocubes with controlled edge length in the range between 18 and 32 nm by taking silver trifluoroacetate as a metal precursor in DEG medium. Fig. 1.11 shows the TEM images of silver nanocubes obtained at different reaction times in DEG. The edge length of silver nanocubes can be tailored by quenching the reaction at different reaction times with the aid of UV-Visible spectrometer. DEG not only serves as a solvent medium but is also responsible for achievement of nucleation in early stage to generate a large number

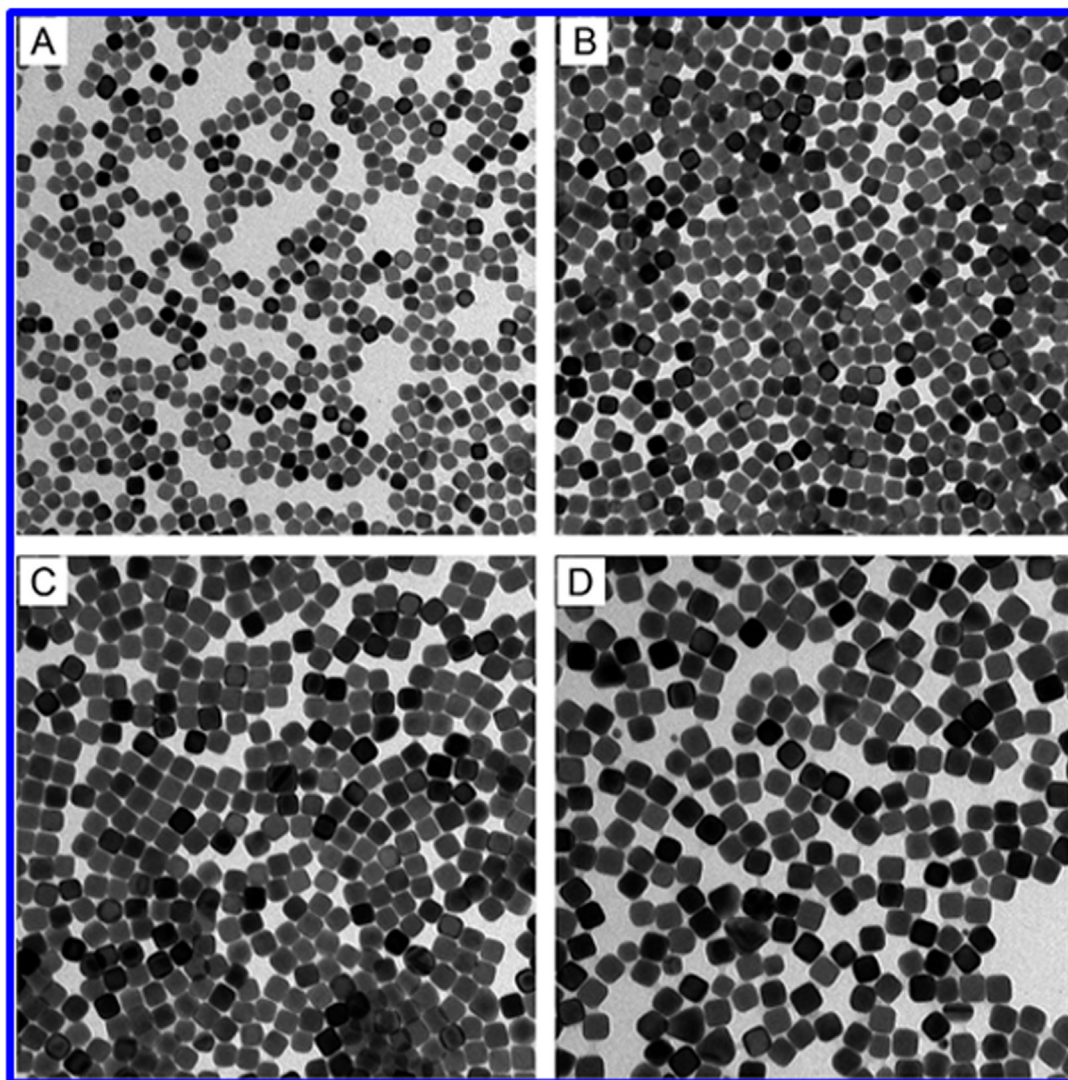


FIGURE 1.11 TEM Images of Ag Nanocubes Obtained at Different Time Intervals in DEG

(A) 30, (B) 60, (C) 120, and (D) 180 min.

Reprinted with permission from Wang, Y., Zheng, Y., Huang, C.Z., Xia, Y., 2013. Synthesis of Ag Nanocubes 18–32 nm in edge length: the effects of polyol on reduction kinetics, size control, and reproducibility. *J. Am. Chem. Soc.* 135, 1941–1951. Copyright 2013, American Chemical Society.

of Ag seeds with slow down the growth rate. The nucleation and growth of the Ag cubes could be monitored by TEM analysis.

Carroll et al. (2011) have extensively studied the effect of polyol for the final morphology of Cu by simple and robust polyol method. Various polyols, such as EG, PG, BG, DEG, and TEG have been utilized with NaOH and methanol. TEM results revealed that the morphology of Cu is strongly

influenced by the nature of the employed polyols that alter the important parameters like nucleation and growth steps during the preparation. Li et al. (2013) developed a straightforward polyol method for the fabrication of Au@Ag heterostructure with nanorod morphology. High quality of Au@Ag heterogeneous nanorods of various aspect ratios were produced by varying the initial concentration of poly(diallyldimethylammonium) chloride (PDDA).

TEM results shown in Fig. 1.12 revealed that the aspect ratios of Au@Ag heterogeneous nanorods are manipulated by the initial concentration of PDDA. The prepared heterogeneous Au@Ag nanorods are stable and found to show size-dependent optical properties, as a result maintained optical properties up to long time.

2.6 SONOCHEMICAL METHOD

The sonochemical method is one of the recently emerged techniques that provide a versatile route to obtain nanostructures for biomedical applications. Fundamentally, it signifies the utilization of high-intensity ultrasounds, which induce transient conditions that are distinct from other conventional synthetic routes like hydrothermal route, spray pyrolysis method, and wet chemical method (Bang and Suslick, 2010; Suslick, 1990; Suslick and Price, 1999). Generally, these transient conditions are generated during the acoustic cavitation, which produce high temperature and high pressure at the center of the bubbles. The bubbles are usually obtained when solutions are exposed to high-intensity ultrasound. The employed conditions in sonochemical method are as follows: (1) speed of sound in liquid should be in the range 1000–1500 ms⁻¹, (2) ultrasonic wavelength is required between 10 cm and 100 μm, and (3) the frequency range of 20 kHz to 15 MHz is necessary. In sonochemical method, two kinds of materials, such as volatile and nonvolatile precursors have been used as starting material for the production of nanomaterials through different reaction mechanisms (Xu et al., 2013). If the volatile compounds are utilized as precursors in sonochemical method, it is called as primary sonochemistry and in case nonvolatile compounds are used, it is termed as secondary sonochemistry. In primary sonochemistry, free metal atoms are generated from volatile organometallic compounds via bond dissociation facilitated by high temperature produced during bubble collapse. The obtained atoms are injected into the liquid phase and subsequent nucleation yielded NPs of various materials in the presence of appropriate template. In the latter case, sonochemical reactions occur even outside of bubble, which undergoes reaction with radicals. The radicals diffuse into liquid, as a result reaction occurs and nanomaterials are generated. By employing this method various metal and metal oxide NPs have been prepared with wide variety of morphologies.

Okitsu et al. (2009) developed an efficient and novel one-pot sonochemical method for the production of Au nanorods via reduction of HAuCl₄ in the presence of AgNO₃, CTAB, and ascorbic acid. Aspect ratio of AuNPs decreased with increasing pH of the solution. Fig. 1.13 illustrates the TEM images of AuNPs formed at different pH values. It was concluded that morphology and aspect ratio of AuNPs are strongly dependent on pH. At higher pH values, spherical-shaped AuNPs with small particle size were formed, whereas, at low pH Au nanorods are exclusively obtained.

2.7 LIQUID-LIQUID INTERFACE METHOD

Liquid–liquid interface strategy is an excellent, simple, and straightforward method to produce nanocrystalline films of metals, metal chalcogenides, and metal oxides by the process of self-assembly at liquid–liquid interface. Self-assembly is a powerful strategy to create novel structures of nanomaterials with great academic interest. The nanomaterial in the form of film is considered important, due to its potential

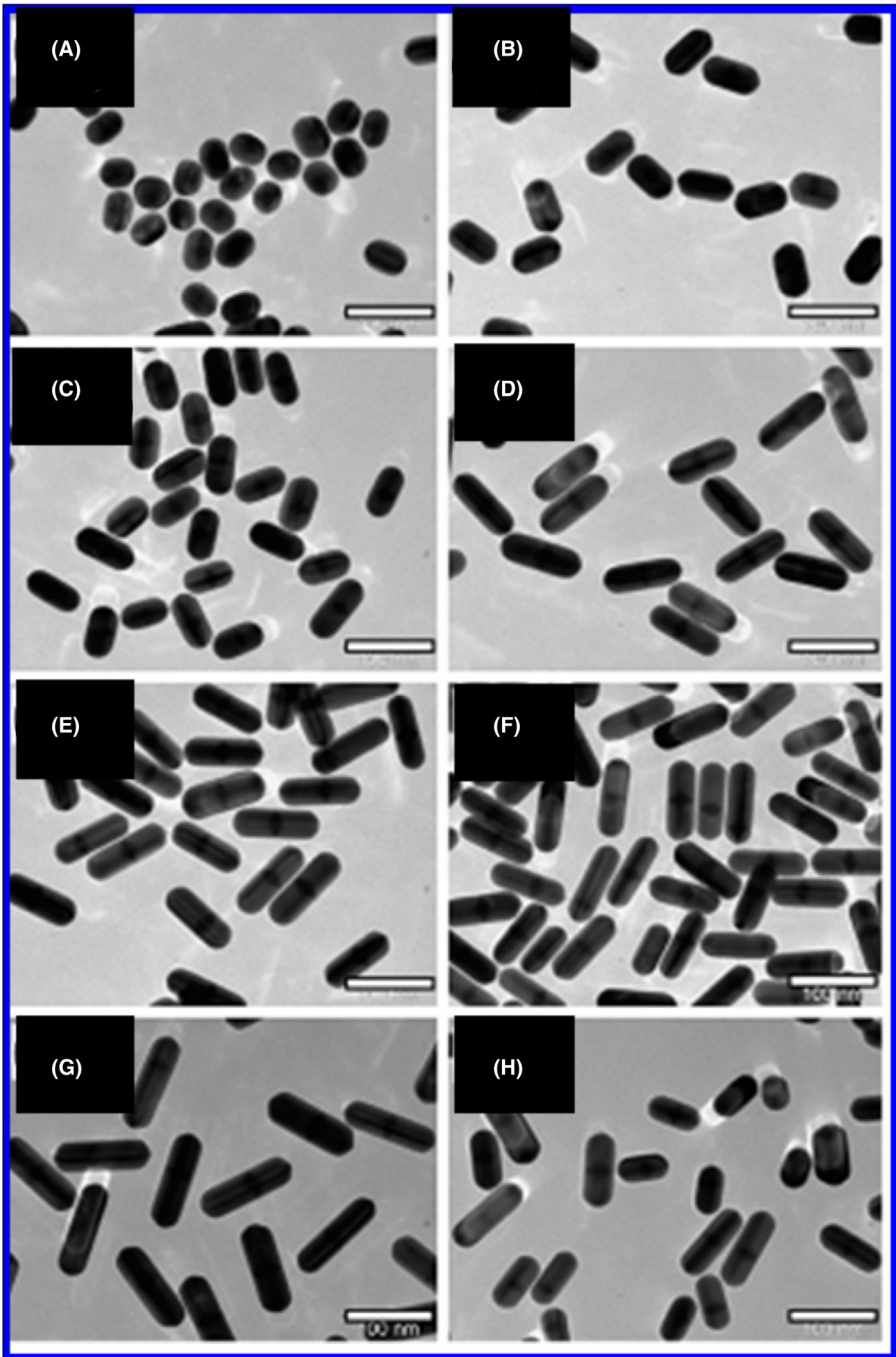


FIGURE 1.12 TEM Image of Au@Ag Heterogeneous Nanorods Obtained at 473 K for 60 h in an EG Solution Containing 0.25 mM HAuCl₄, 2.5 mM AgNO₃, and Different PDPA Concentrations

(A) 5, (B) 10, (C) 15, (D) 20, (E) 25, (F) 30, (G) 35, and (H) 40 mM. All scale bars are 100 nm.

Reprinted with permission from Li, C., Sun, L., Sun, Y., Teranishi, T., 2013. One-pot controllable synthesis of Au@Ag heterogeneous nanorods with highly tunable plasmonic absorption, *Chem. Mater.* 25, 2580–2590. Copyright 2013, American Chemical Society.

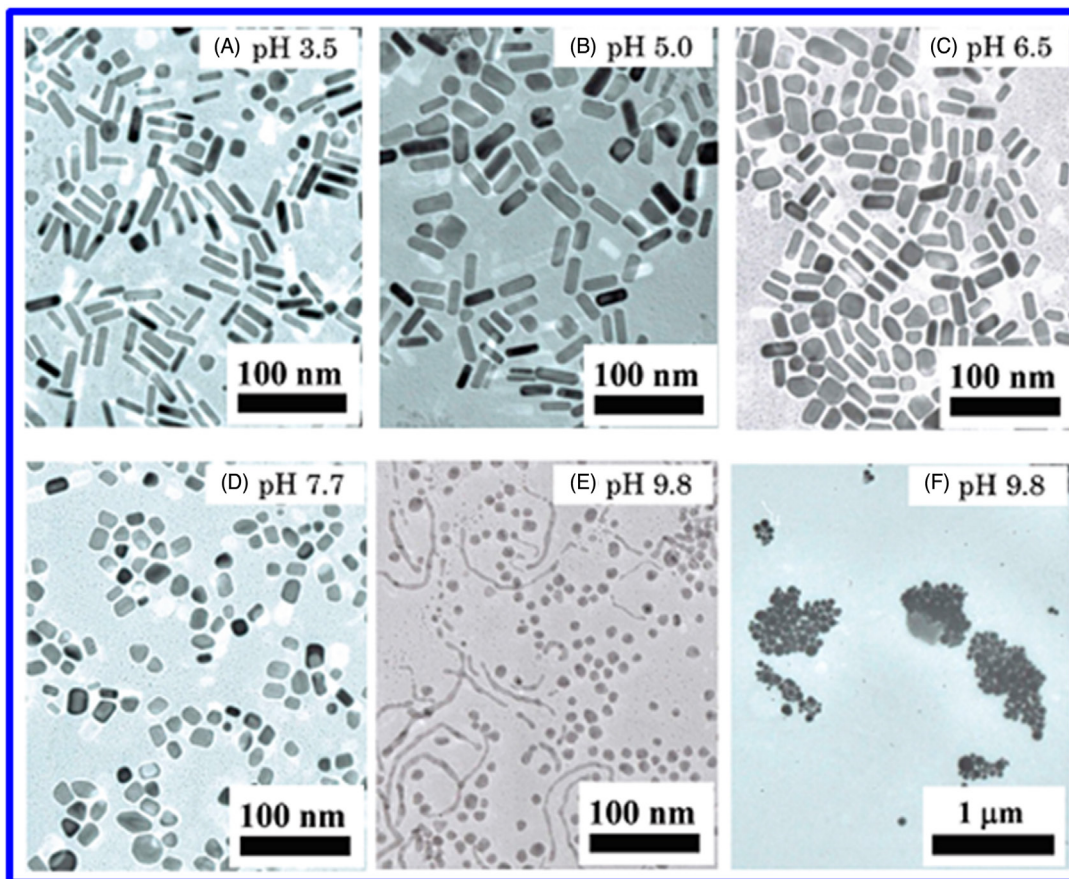
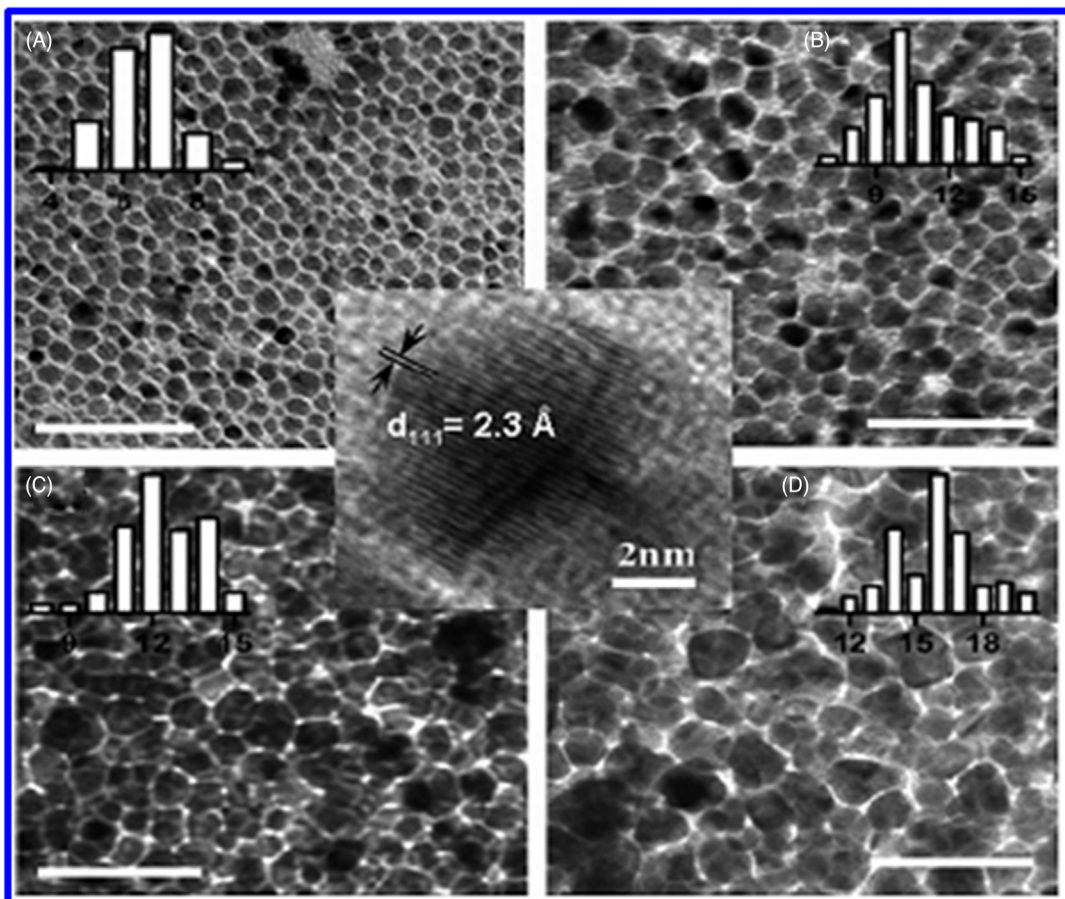


FIGURE 1.13

TEM images of Au nanorods and particles formed in different pH solutions of (A) pH 3.5, (B) pH 5.0, (C) pH 6.5, (D) pH 7.7, (E) pH 9.8 after 180 min irradiation under argon. (F) TEM images of AuNP formed at a pH 9.8 solution at 180 min standing without ultrasonic irradiation.

Reprinted with permission from Okitsu, K., Sharyo, K., Nishimura, R., 2009. One-pot synthesis of gold nanorods by ultrasonic irradiation: the effect of pH on the shape of the gold nanorods and nanoparticles. Langmuir 25, 7786–7790. Copyright 2009, American Chemical Society.

application in nanodevices (Rao et al., 2003). This method generally proceeds through a single step to form nanocrystalline films at the interface of two immiscible liquids, where one liquid is water and the other one is organic liquid. The interface is nonhomogeneous, usually has the thickness of a few nanometers, and offers an excellent path for the self-assembly and chemical manipulation of nanocrystals. In this method, metal precursors are taken in organic layer, which on reaction with appropriate reagent containing aqueous layer formed an ultrathin nanocrystalline film at the interface by self-assembly process. The obtained film was readily transferred on solid substrate by using an appropriate solvent. The film was broken into hydrosol or organosol for further characterization studies. The interfacial energy of the

**FIGURE 1.14**

TEM image of ultrathin nanocrystalline Au films obtained at the liquid–liquid interface at (A) 303, (B) 318, (C) 333, and (D) 348 K. Histograms of particle size distribution are shown in insets. All scale bars are 50 nm. A high-resolution image of an individual particle is shown at the center.

Reprinted with permission from Agrawal, V.V., Kulkarni, G.U., Rao, C.N.R., 2005. Nature and properties of ultrathin nanocrystalline gold films formed at the organic-aqueous interface. J. Phys. Chem. B. 109, 7300–7305. Copyright 2005, American Chemical Society.

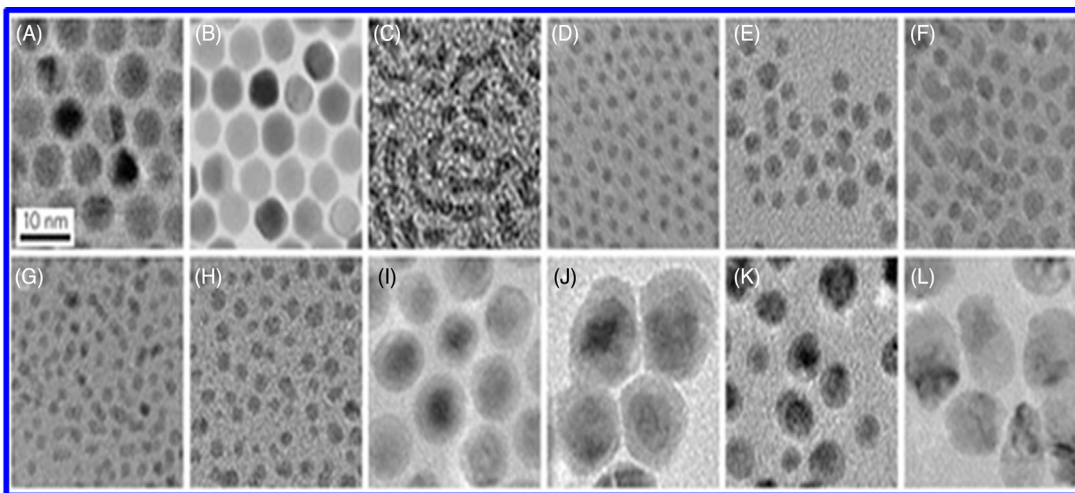
assembly process at liquid–liquid interface is influenced by the following factors: (1) nature of the interface, (2) alteration of surface of the NPs at interface, and (3) the effective radius of the NPs, smaller NPs are weakly attached to the interface than larger particles ([Rao and Kalyanikutty, 2008](#)). Rao et al. have proposed and developed a facile one-pot liquid–liquid interface method for the fabrication of a variety of noble metal NPs ([Fig. 1.14](#)) ([Agrawal et al., 2005](#)). The preparation of nanocrystalline ultrathin Au films was carried out by taking appropriate concentration of corresponding metal precursor Au (PPh_3Cl) in toluene, later allowed to contact with aqueous solution containing NaOH at 300 K. After the formation of two layers, tetrakishydroxy-methylphosphonium chloride (THPC) which is acting as a reducing

agent was injected; as a result yellowish colored transparent Au nanocrystalline film was formed at the liquid–liquid interface, which was thoroughly characterized by employing XRD, transmission electron microscopy, and so on. According to their study, various parameters significantly influenced the formation of nanocrystalline Au films. In this respect, temperature profoundly affected the particle size of Au film and the mean diameter of particles increased with respect to employed temperature. The effect of temperature on the size distribution of film is shown in Fig. 1.8. In addition, concentration of metal precursor played a crucial role in terms of quality, stability, and thickness of the film. Furthermore, the electronic properties of the resulted Au film could be affected by the reaction temperature. In addition to Au, it is possible to produce nanocrystalline films of other metals, such as Ag, Cu, and Pd at the interface by adopting liquid–liquid interface strategy (Rao et al., 2003).

The nanocrystalline films are obtained by taking respective precursors, such as $\text{Ag}_2(\text{PPh}_3)_4$, $\text{Cu}(\text{PPh}_3)\text{Cl}$, and palladium acetate in the organic layer and appropriate reducing agent in aqueous layer. Nanocrystalline films of binary and ternary alloys, such as Au–Ag, Au–Cu and Au–Ag–Cu have been generated at toluene–water interface by taking mixtures of corresponding metal precursors and reducing agents (Agrawal et al., 2006). The nature of the reducing agent showed noticeable effect on the morphology of the final nanocrystalline film.

2.8 PHASE-TRANSFER METHOD

Phase-transfer method is a widely used synthetic technique to produce metal NPs. Phase-transfer method represents a good approach to prepare size and shape-tunable metal NPs. This method involves the transfer of reactant from polar medium to nonpolar medium and vice versa (Rao et al., 2012). However, the transfer of metal NPs to organic medium is an excellent approach; because, yield of NPs in aqueous phase suffers from several drawbacks. Whereas, preparation of metal NPs directly in nonpolar organic medium was limited due to poor solubility of the corresponding metal precursors. Therefore, phase transfer of metal NPs in aqueous phase to nonpolar organic phase has few advantages, such as avoiding the use of organometallic precursor, lowering of interfacial energy, and use of relatively high concentrations thereby producing narrow size distribution of particles with controllable morphologies (Yang et al., 2011). Brust et al. (1994) were the first to report the alkanethiol-capped AuNPs by adopting phase-transfer method using tetraalkylammonium bromide as the phase-transfer agent. This method involves the phase transfer of chloroaurate ions into toluene in presence of a phase-transfer agent, followed by the subsequent reduction of gold ions by NaBH_4 yielding 1–3 nm sized capped AuNPs with homogeneous size distribution. A simple and efficient phase-transfer method was developed for the preparation of AOT-capped AgNPs, which are highly dispersible in both aqueous and organic solvents. Initially hydrophilic AOT-capped AgNPs are prepared by the reduction of corresponding silver precursor. The resulting aqueous AgNPs are readily transferred to organic phase (cyclohexane) by the aid of phosphoric acid. The concentration of surfactant played vast effect on the particle size of AOT-capped aqueous AgNPs (Prasad et al., 2005). Phase transfer of Pt, Au, and AgNPs to organic phase was achieved by simple phase-transfer technique. The size and morphology of metal NPs before and after phase transfer was thoroughly examined by TEM analysis. Some interesting findings were revealed from TEM analysis; those are, the particle size and shape of Pt didn't change after phase transfer, whereas Ag showed slight variations in the particle size after phase transfer. However, gold showed a variety of morphologies with different particle size (Feng et al., 2006). Yang et al. (2009) have demonstrated a protocol for phase

**FIGURE 1.15**

(A) AgNPs derived with HDD, (B) Au, (C) warm like Pd and, (D) Pt from Pt (IV), obtained with TBAB, (E) Ag–Au, (F) Pd–Pt, (G) Pt–Rh, (H) Pt–Ru alloy NPs synthesized by coreduction of the metal precursors with TBAB. (I) 7.4 nm Au@Ag, (J) 12.7 nm Au@Ag, (K) 3.9 nm Pt@Ag, and (L) 9.2 nm Pt@Ag core–shell NPs prepared by seed-mediated growth.

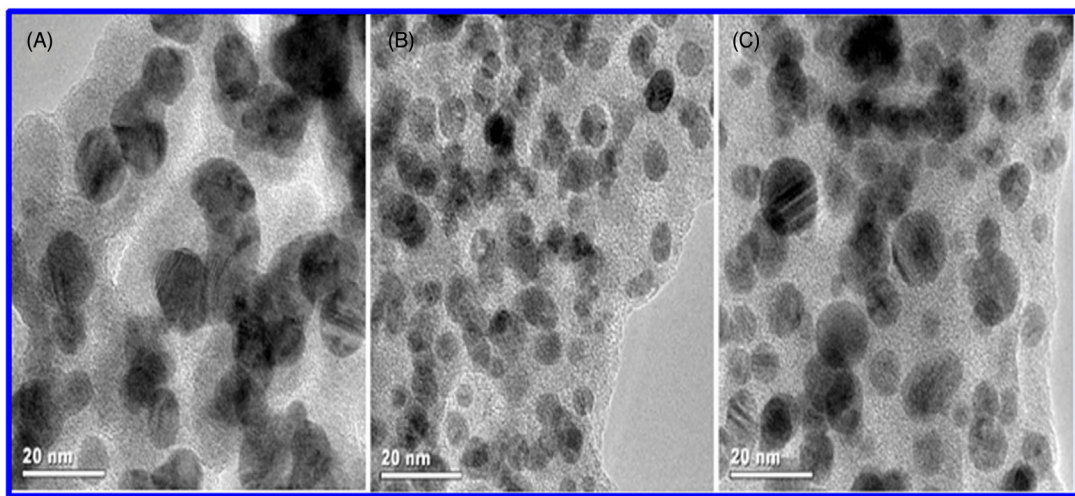
Reprinted with permission from Yang, J., Sargent, E., Kelley S., Ying, J.Y., 2009. A general phase-transfer protocol for metal ions and its application in nanocrystal synthesis. Nat. Mater. 2009, 8, 683. Copyright 2009, Nature Publishing Group.

transfer of various metal ions to organic medium for the production of NPs (Fig. 1.15). The presence of ethanolic dodecylamine (DDA) solution can facilitate the transfer of metal ions from aqueous phase to organic medium.

2.9 BIOSYNTHESIS METHOD

Till date numerous methods including physical and chemical methods have been developed for metal NP synthesis in bulk quantities. However, these methods, usually, often use toxic chemicals, drastic conditions, and additives. Therefore, development of reliable, biocompatible, and green method for the production of metal NPs has gained more attention from the scientific community (Jain et al., 2011).

In this context, biosynthesis of metal NPs using plant extract or plant tissue or living plant has opened new opportunity in the production of NPs in large-scale quantities. Biosynthesis approach is an environmental friendly, cost effective, and fast method, which avoids the use of harsh conditions, toxic reagents, and expensive chemicals. Few challenges have been encountered in the biosynthesis method for production of NPs that are of the size and shape of the NPs. Njagi et al. (2011) have demonstrated a simple, one-step biosynthetic method for the preparation of Ag and FeNPs using aqueous sorghum bran extract as the reducing and capping agent at room temperature. The corresponding metal precursors are reduced to respective metal ions by the assistance of aqueous sorghum bran extract producing 10-nm AgNP with face-centered cubic structure and 50-nm diameter FeNPs. The phenolic compounds presented in sorghum bran extract can be used as reducing as well as capping agents during the formation

**FIGURE 1.16**

TEM images of AgNPs prepared by sorghum bran extract at (A) 25, (B) 50, and (C) 80°C.

Reprinted with permission from Njagi, E.C., Huang, H., Stafford, L., Genuino, H., Galindo, H.M., Collins, J.B., Hoag, G.E., Steven, L.S., 2011. Biosynthesis of iron and silver nanoparticles at room temperature using aqueous sorghum bran extracts. *Langmuir* 27, 264–271. Copyright 2011, American Chemical Society.

of NPs. The phenolic compounds exhibit several advantages, such as water solubility, nontoxicity, and biodegradability and offer green synthetic route for the preparation of metal NPs. Fig. 1.16 shows the TEM images of AgNPs synthesized at different temperatures. TEM analysis revealed the formation of uniform size spherical AgNPs. As prepared FeNPs are examined for bromothymol degradation. [Shiv Shankar et al. \(2003\)](#) have reported different shapes of AuNPs by exposing the geranium leaves and its endophytic fungus *colletotrichum* sp. to chloroaurate. The rapid reduction of respective metal ions had taken place by terpenoids present in the geranium leaves; whereas, polypeptides or enzymes in *colletotrichum* sp. were responsible for the reduction resulting in the formation of AuNPs. The TEM results of AuNPs obtained by both the sources provided excellent features. The AuNPs synthesized by using fungus were spherical in shape whereas in case of geranium leaves different morphologies including rods, flat sheets, and triangles were obtained. The crucial reaction parameters, such as temperature, pH, and reaction time profoundly influenced the size and shape of the final nanomaterial. It is obvious from the literature that, pH may play a crucial role in controlling the size and morphology of NPs. [Castro et al. \(2011\)](#) reported that the morphology of AuNPs obtained by sugar beet pulp was highly dependent on the pH. The size and shape of the NPs with respect to pH was examined by UV-Vis spectroscopy and TEM study. At, pH 9 smaller NPs with 10-nm diameter were obtained and with gradual increase of pH to 10, rod-like shape was achieved. Finally, nanowire shape was attained by adjusting pH to 11. [Sathishkumar et al. \(2009\)](#) reported the production of PdNPs by reduction of palladium chloride using *Cinnamomum zeylanicum* bark extract as biomaterial. They found that, temperature shows a notable effect on the particle size but not on the morphology. [Li et al. \(2007\)](#) studied the effect of reaction time on the preparation of AgNPs by treating silver ions with *Capsicum annuum* L. extract. A spherical-shaped

NP with small size was obtained at 5 h, with gradual increase of reaction time to 9 and 11 h, particle size increased and showed crystalline and polycrystalline morphology, respectively for AgNPs. Therefore, it is believed that, reaction time played a significant effect on the shape and size of the particles.

2.10 TEMPLATE-DIRECTED SYNTHETIC METHOD

The template-directed method is practically a straightforward method for the production of high-quality novel metal and metal oxide NPs through the mediation of appropriate template. The template is generally used to manipulate the formation and growth of the NPs with desired morphology. Importantly pore size, grain morphology, phase composition, and size of the nanomaterial can be improved by employing suitable template material. In this method, the solid product is formed over the sacrificial template via the liquid–solid interfacial reaction (Bao et al., 2014). The main function of the template is to provide a desired morphology, which is similar to that of template morphology to the final nanomaterial during the synthetic procedure. Additionally, template-directed method offers several benefits, such as lower reaction temperature, shorter reaction time, less requirement of toxic precursors and solvents resulting in nonformation of toxic-side products, and the use of external energy source can be avoided (Patete et al., 2011). Production of preferred nanostructures within the template and the complete removal of template material by suitable routes, such as chemical etching and calcination are the crucial steps in the aforementioned method. Generally, template methodology can be categorized as hard and soft template approaches based on their structure. Hard templates usually are porous silica, porous carbon, porous anodic alumina, polystyrene beads, block polymers, carbon NPs, metals, metal oxides, and mica. On the other hand, emulsion droplets, surfactant micelles, polymer vesicles, bubbles, and amphiphilic surfactants are often adopted as soft templates. However, in most of the cases, template method is associated with a major drawback that the template employed in the process must be completely removed at the end of the synthesis, which rigorously affects the purity of the resulted nanomaterial and makes the process very complicated.

ZnO hollow spheres were fabricated by a novel and simple method with the use of sulfonated polystyrene core–shell spheres as template (PS) (Deng et al., 2008). In a typical approach, requisite quantity of $\text{Zn}(\text{Ac})_2 \cdot 2\text{H}_2\text{O}$ was mixed with ethanol solution containing sulfonated polystyrene core–shell (PS) template; as a result, Zn ions adhered on the surface of template spheres through the electrostatic interaction. Once NaOH was added to the above mixture, the Zn ions readily reacted with NaOH to form ZnO crystal nuclei, which was followed by the formation of ZnO nanoshells. Afterward, the template spheres were dissolved in the same solution to produce ZnO hollow spheres. A systematic analysis for the formation of ZnO hollow spheres was undertaken by varying the reaction parameters, such as concentration of NaOH, concentration of $\text{Zn}(\text{Ac})_2 \cdot 2\text{H}_2\text{O}$, and size of templates employed. TEM images of ZnO hollow spheres prepared by different NaOH concentrations showed that lower NaOH concentration either deformed or broke the ZnO hollow spheres (Fig. 1.17). However, NaOH here played a dual role: assisted the formation of ZnO hollow spheres as a reactant and helped to dissolve the template spheres. On the other hand, the concentration of $\text{Zn}(\text{Ac})_2 \cdot 2\text{H}_2\text{O}$ showed a significant effect on the wall thickness of the ZnO hollow spheres. At lower concentrations, very thin hollow spheres were obtained, whereas, increase of the concentration enhanced the wall thickness tremendously; but some aggregated ZnONPs were also observed along with the spheres. Therefore, it was proved that the variation in the concentration of $\text{Zn}(\text{Ac})_2 \cdot 2\text{H}_2\text{O}$ could facilitate the changes in the wall thickness of ZnO hollow spheres obtained in the course of reaction. The synthesized ZnO hollow spheres were examined for

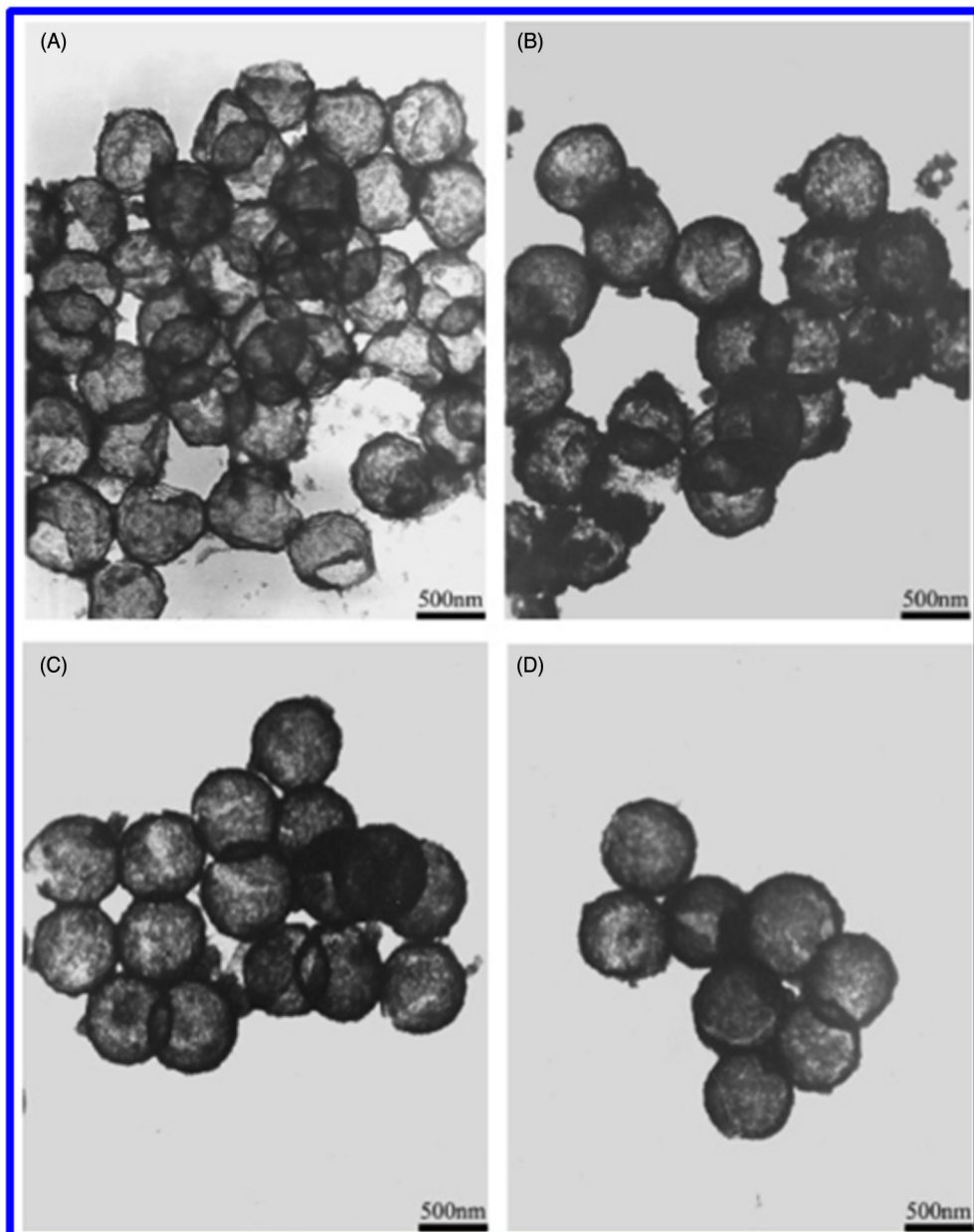


FIGURE 1.17 TEM Images of ZnO Hollow Spheres Prepared by Various NaOH Concentrations

(A) 0.025 mol/L, (B) 0.1 mol/L, (C) 0.3 mol/L, (D) 0.4 mol/L, and $\text{Zn}(\text{Ac})_2 \cdot 2\text{H}_2\text{O}$: 0.036 mol/L.

Reprinted with permission from Deng, Z., Chen, M., Gu, G., Wu, L., 2008. A facile method to fabricate ZnO hollow spheres and their photocatalytic property. *J. Phys. Chem. B* 112, 16–22. Copyright 2008, American Chemical Society.

photocatalytic activity and found to show excellent catalytic performance. Interestingly, the size of the template employed had significant control over the size of the ZnO hollow sphere.

Gundiah et al. (2003) have prepared a variety of oxide nanotubes, such as TiO₂, ZrO₂, WO₃, and ZnO by employing tripodal cholamide-based hydrogel as template. For example, nanotubes are synthesized by taking tetrabutyl orthotitanate (TBOT) as titanium source and the synthetic method involves hydrolysis of the titanium precursor in the presence of template followed by deposition of TiO₂ on the surface of the template and removal of the template material. The TEM analysis revealed the formation of TiO₂ nanotubes with 4–7 nm and 10–20 nm inner diameter and outer diameter, respectively. Similarly, ZrO₂, WO₃, and ZnO nanotubes with desired diameter can be easily synthesized by adopting the aforementioned procedure in the presence of tripodal cholamide-based hydrogel template. Irrespective of metal oxide nanotubes, all are produced with excellent yields in the course of the reaction. Apart from the metal oxide nanotubes, a variety of metal oxide nanorods, such as V₂O₅, WO₃, MoO₃, RuO₂, IrO₂, and Sb₂O₅ were prepared by the same group employing carbon nanotube as template agent. Interestingly, the obtained metal oxide nanotubes are longer than the carbon nanotube template (Satishkumar et al., 2000).

Bao et al. (2014) have developed an efficient template-assisted method for synthesis of CeO₂@Cu₂O nanocomposites, employing Cu₂O cubes and octahedra as the sacrificial template materials. The morphologies of the CeO₂@Cu₂O nanocomposites were examined by transmission electron microscopy (TEM) and scanning electron microscopy (SEM). Fig. 1.18 shows the TEM and SEM images of CeO₂@Cu₂O nanocomposites.

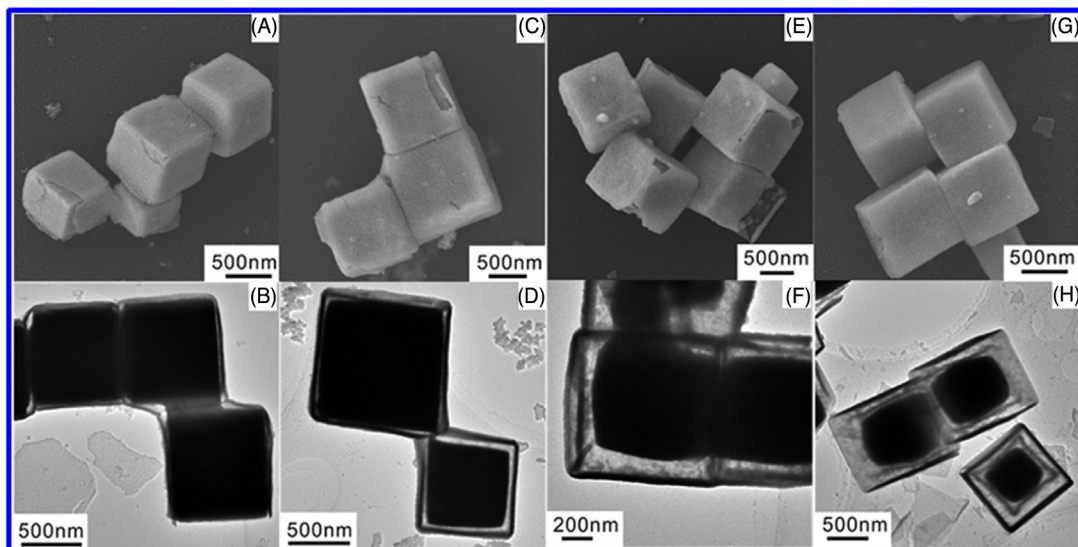


FIGURE 1.18

SEM and TEM images of (A–B) CeO₂@c-Cu₂O-0.045, (C–D) CeO₂@c-Cu₂O-0.09, (E–F) CeO₂@c-Cu₂O-0.18, and (G–H) CeO₂@c-Cu₂O-0.36.

Reprinted with permission from Bao, H., Zhang, Z., Hua, Q., Huang, W., 2014. Compositions, structures, and catalytic activities of CeO₂@Cu₂O nanocomposites prepared by the template-assisted method. Langmuir 30, 6427–6436. Copyright 2014, American Chemical Society.

SEM images demonstrated that $\text{CeO}_2@\text{Cu}_2\text{O}$ nanocomposites with various compositions exhibited cubic nanostructure, whereas, TEM analysis demonstrated the cubic core/shell nanostructure for $\text{CeO}_2@\text{Cu}_2\text{O}$ nanocomposites. The cubic core had shrunk with respect to the increase in Ce content, thereby enhancing the space between the shell and the core, which is clearly shown in the Fig. 1.18. The resulting $\text{CeO}_2@\text{Cu}_2\text{O}$ nanocomposites were examined for CO oxidation and the activity is highly dependent on their composition and structure.

Formation of triangular Ag nanoplates was achieved by the reduction of Ag ions with ascorbic acid in the presence of a soft template (CTAB) (Chen and Carroll, 2002). The resulting particles had an average edge size of 8 nm, thickness of 24 nm, and the degree of truncation of 0.35. Particles with different morphologies like rods, discs, spheres, cubes, tetrahedral, and squares were detected. Liu et al. (2005) have prepared the hierarchical iron oxide with controllable porous structure with the assistance of wood template. Hierarchical iron oxide nanostructures with a pore size of 20 nm to 50 μm were prepared by taking inorganic precursor solution in wood template. The structural property of hierarchical iron oxide was investigated with the help of various characterization techniques, such as SEM, FESEM, EDAX, XRD, and TEM. Moreover, the pore-size distribution of wood-templated hierarchical iron oxide was controlled by varying the calcination temperature as well as nature of template. Metal oxide nanostructures were fabricated with the aid of porous carbonaceous coating and multiwalled carbon nanotube core as dual template. Variety of metal oxide nanostructures were fabricated with the utility of porous carbonaceous coating and multiwalled carbon nanotube core as dual templates (Zhang et al., 2010a). For example, the preparation of SnO_2 , ZrO_2 , Fe_2O_3 , and CeO_2 hollow nanostructures involves multiple key steps. The initial step comprises the coating of carbonaceous layer over the surface of the nanotube, to form a dual template during the thermal treatment. Then the metal cations were allowed to be adsorbed on the dual template followed by removal of the carbonaceous layer by calcination, at relatively lower temperature, resulting in the formation of MWCNTs@MO composite. The prepared composite was subsequently subjected to calcination at 550°C to remove the MWCNTs, resulting in the production of hollow structured metal oxides.

3 APPLICATION OF METAL NANOPARTICLES IN THERANOSTICS

Theranostics is a new and innovative process in the field of cancer therapy. It combines multiple steps of the therapeutic system, such as therapy, diagnosis, and monitoring of therapy by imaging (Fig. 1.19). Theranostics provides a means to follow up the success rate of the therapy in individual patients by imaging the tumors throughout the entire period of treatment. The metal NPs exhibiting physical properties, such as, plasmonic resonance and fluorescent enhancement and chemical property of catalytic activity enhancement provide the suitable means of targeting and drug delivery simultaneously.

3.1 DIAGNOSIS AND DRUG DELIVERY

Nanoscale structures can exhibit widely different properties to bulk materials or small molecules, which renders them applicable in the fields of medical imaging. AuNPs, such as rods or shells exhibit strikingly strong fluorescence with a quantum yield of up to 10^{-3} (Payne et al., 2006). Such fluorescence can be readily applied in the biomedical field, especially as it can be tuned to the NIR window (650–900 nm) by changing nanostructure size and morphology. Tissue absorbs light weakly in the

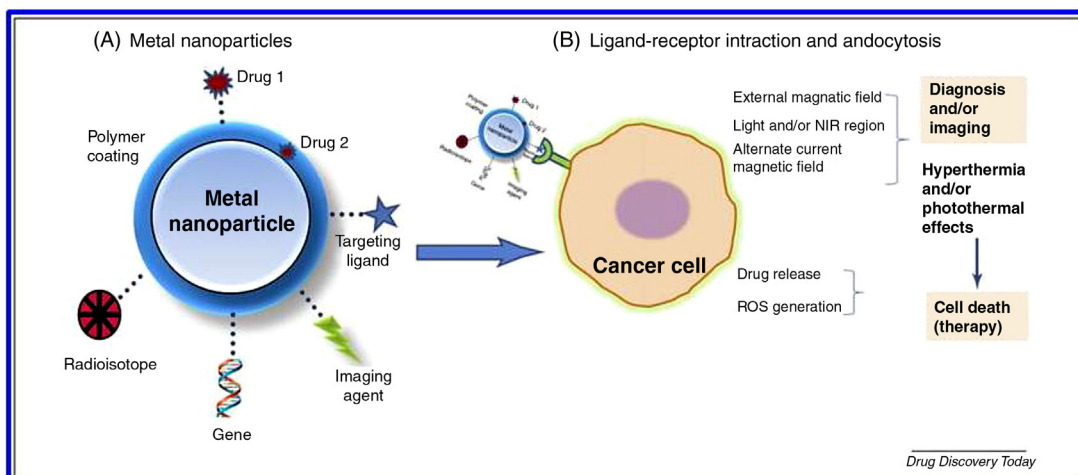


FIGURE 1.19 Designing Multifunctional Metal NPs for Cancer Therapy

(A) Conjugation of drugs molecules over the metal NP surface of particles using chemical functional groups present on the surface of particle or on the coated polymeric matrix. (B) Interaction of Particles with cancer cells via ligand–receptor interactions, and endocytosis.

Reprinted with permission from Sharma, H., Mishra, P.K., Talegaonkar, S., Vaidya, B., 2015. Metal nanoparticles: a theranostic nanotool against cancer. *Drug Discov. Today* 20, 1143–1151. Copyright 2015, Science Direct.

NIR window, making this window ideal for optically based applications (Zhang et al., 2010b). AuNPs absorb X-rays strongly and can thus be used as contrast agents for X-ray based imaging techniques and as adjuvants for radiotherapy (Galper et al., 2012).

Qian et al. (2015) have demonstrated the use of TiS₂–PEG (titanium sulfide–polyethylene glycol) nanosheet as a photothermal agent for in vivo cancer treatment. Mice bearing 4T1 tumors were injected with a TiS₂–PEG solution (2 mg/mL, 200 μL) or saline as the control was exposed to an 808-nm laser at a power density of 0.8 W/cm² for 5 min at 24 h postinjection. Owing to the strong NIR absorbance and efficient tumor accumulation of TiS₂–PEG, the tumor temperatures of mice injected with TiS₂–PEG quickly increased to ~65°C within 5 min under NIR laser irradiation (Fig. 1.20). In contrast, the surface temperature of tumors in mice injected with saline showed little change under the same irradiation conditions (Qian et al., 2015).

Another highly useful feature is the electromagnetic field enhancement by sharp and spiky edges of the nanostructures, such as stars or nanorods, which can be used in surface-enhanced Raman spectroscopy imaging (von Maltzahn et al., 2009). Fleischmann et al. (1974) showed that Raman signals from different molecular sources can be enhanced by their adsorption on silver metal surface. Later, the same was found with other metals as well. Since then, metal NPs mostly gold and silver were employed in surface-enhanced Raman scattering (SERS), leading to the development of a wide variety of new biosensors for detection of biomolecules (Rycenga et al., 2009). Afterward, conjugated noble metal NPs were also introduced in SERS-based biosensors.

Metal and metal oxide NPs are being actively investigated as carriers for targeted drug delivery in cancer therapeutics (Dobson, 2006). They are designed to contain tumor-targeting ligands that bind to

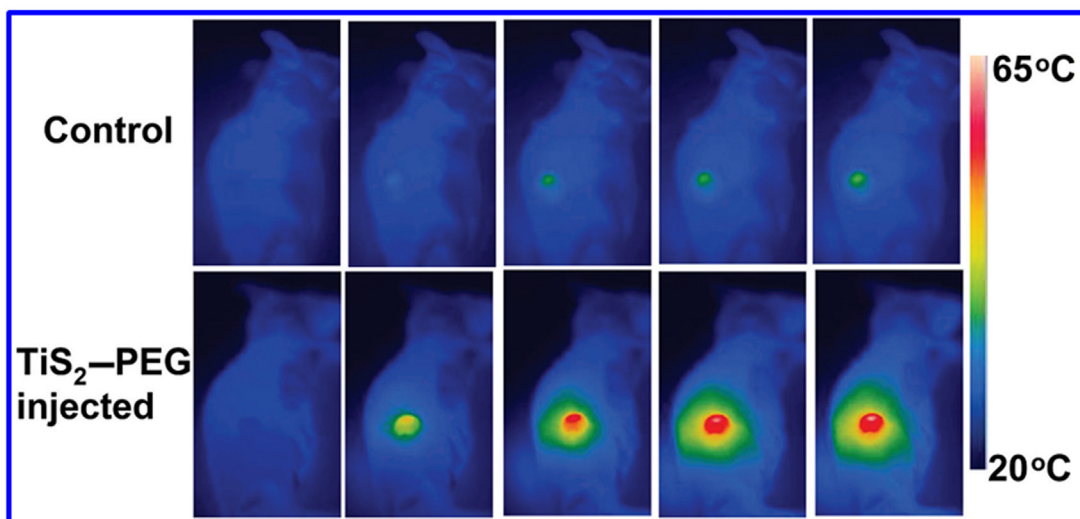


FIGURE 1.20 Infrared Thermal Images of 4T1 Tumor-Bearing Mice With i.v. Injection of a TiS_2 -PEG Solution (2 mg/mL, 200 μL) Under Laser Irradiation at a Power Density of 0.8 W/cm² for 5 min (24 h Postinjection)

Reprinted with permission from Qian, X., Shen, S., Liu, T., Cheng, L., Liu, Z., 2015. Two-dimensional TiS_2 nanosheets for in vivo photoacoustic imaging and photothermal cancer therapy. *Nanoscale* 7, 6380–6387. Copyright 2015, Royal Society of Chemistry.

particular cells within the tumor to fasten the NP within solid tumor. In this way, metallic NP drug-delivery systems are capable of sequestering anticancer drugs exclusively within the tumor and thereby reduce the accumulation of drugs in healthy organs. Their large surface area-to-volume ratio provides a surface for chemical modification, which can improve cell entry, protect the therapeutic agent in the biological milieu, and improve bioavailability of the anticancer agent (Moghimi and Patel, 1998). For example, Zhang et al. have reported multifunctional mesoporous silica NPs for cancer-targeted and controlled drug delivery, which have three components—the mesoporous silica NP core, the amino-b-cyclodextrin, and the PEG polymers functionalized with an adamantane (Ad) unit at one end and a folate (FA) unit at the other end (Ad-PEG-FA). The surface of mesoporous silica NPs is first functionalized with amino-b-cyclodextrin rings bridged by cleavable disulfide bonds, blocking drugs inside the mesopores of the NPs.

The Ad-PEG-FA polymers are immobilized onto the NP surface through strong b-cyclodextrin/adamantane complexation. The multifunctional NPs can be efficiently trapped by folate-receptor-rich cancer cells through receptor-mediated endocytosis, where they then rapidly release the loaded anticancer drug (Zhang et al., 2012). AuNP targeting can be achieved in a passive fashion, where long circulating AuNPs can accumulate in cancerous tissues by penetrating the leaky tumor vasculature. This is known as the enhanced permeability and retention (EPR) effect (Maeda et al., 2000). Alternatively, AuNPs can be targeted to specific cell types, receptors, or proteins via attachment of targeting ligands, such as antibodies, proteins, peptides, aptamers, and small molecules (Fig. 1.21) (Cormode et al., 2008). Thus far, Doxil and Abraxane are the most successful nanotechnology-based treatments in the world market. Both nanocarriers showed reduction of the toxicity allowing for elevated doses (Nichols and Bae, 2012).

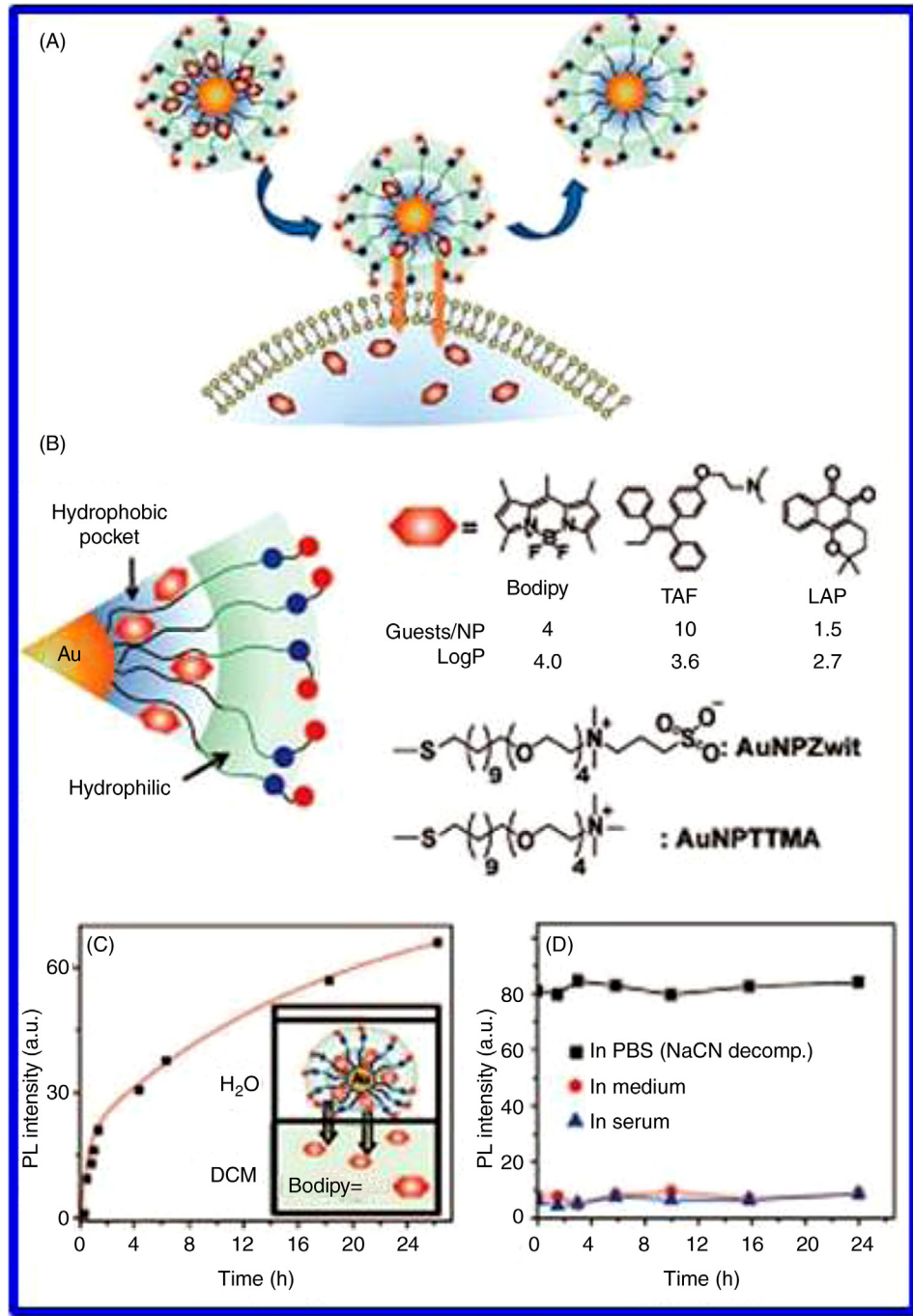


FIGURE 1.21

(A) Delivery of payload to cell through monolayer–membrane interactions. (B) Structure of particles and guest compounds: Bodipy, TAF, and LAP, the number of encapsulated guests per particle, and log P of the guests. (C) Release of Bodipy from AuNPZwit-Bodipy in DCM-aqueous solution two-phase systems ($\lambda_{\text{ex}} = 499$ nm; $\lambda_{\text{em}} = 517$ nm). (D) PL intensity of AuNPZwit-Bodipy in cell culture medium and 100% serum, indicating little or no release relative to AuNPZwit-Bodipy in PBS after NaCN-induced release of guest molecules ($\lambda_{\text{ex}} = 499$ nm; $\lambda_{\text{em}} = 510$ nm).

Reprinted with permission from Kim, C.K., Ghosh, P., Pagliuca, C., Zhu, Z.-J., Menichetti, S., Rotello, V.M., 2009. Entrapment of hydrophobic drugs in nanoparticle monolayers with efficient release into cancer cells. *J. Am. Chem. Soc.* 131, 1360–1361.

Copyright 2009, American Chemical Society.

4 CONCLUSIONS

The past couple of decades have witnessed an exponential growth of activities in the field of nanotechnology worldwide, which came up with the hope of diverse possible applications in pharmacy and biotechnology. A wide range of synthesis methods have been studied so far to fabricate various metal and metal oxide NPs. Mainly, wet chemical approaches offer potential reaction pathways to obtain better materials in terms of chemical homogeneity and size-tunable properties. Nevertheless, it is difficult to separately control the crystallization, surface structure, and agglomeration of particles. Biosynthetic techniques are also being explored. This method is superior in terms of toxicity and deduction of use of hazardous chemicals in synthesis; although challenges regarding size and shape controllability are yet to be achieved.

However, understanding of metal NP toxicity is also necessary with the rapid growth of this field. The normal mode of action of metal NPs is the production of ROS. Excessive oxidative stress is harmful and can lead to atherosclerosis, pulmonary diseases, and further cancers. The toxicity of metal NPs can be subdued by targeting the specific target site. Or else, alternative approaches like application of biodegradable polymers as reducing and functionalizing agents, can also suppress the toxicity of metal NPs. Hence, before their clinical trial several factors have to be settled, which include preparation method, reproducibility and stability of the metal NPs, etc. More importantly, the safe level of application, extent of accumulation of metal NPs in the patient body, and their toxicological effects in the long run are to be considered very seriously. However, once these problems are sorted out, metal NPs can become a potential clinical weapon to fight against serious illness.

ACKNOWLEDGMENTS

We wish to specially acknowledge all the researchers whose work is described in this chapter for their valuable contributions. B.G and D.M thank the Council of Scientific and Industrial Research (CSIR), New Delhi for the research fellowships. Financial support for this project was received from the Department of Science and Technology, New Delhi, under SERB Scheme (SB/S1/PC-106/2012).

REFERENCES

- Aden, A.L., Kerker, M., 1951. Scattering of electromagnetic waves from two concentric spheres. *J. Appl. Phys.* 22, 1242–1246.
- Agrawal, V.V., Kulkarni, G.U., Rao, C.N.R., 2005. Nature and properties of ultrathin nanocrystalline gold films formed at the organic-aqueous interface. *J. Phys. Chem. B* 109, 7300–7305.
- Agrawal, V.V., Mahalakshmi, P., Kulkarni, G.U., Rao, C.N.R., 2006. Nanocrystalline films of Au-Ag, Au-Cu, and Au-Ag-Cu alloys formed at the organic-aqueous interface. *Langmuir* 22, 1846–1851.
- Alexander, J.W., 2009. History of the medical use of silver. *Surg. Infect.* 10, 289–292.
- Ba, J., Polleux, J., Antonietti, M., Niederberger, M., 2005. Nonaqueous synthesis of tin oxide nanocrystals and their assembly into ordered porous mesostructures. *Adv. Mater.* 17, 2509–2512.
- Bandyopadhyay, S., Peralta-Videa, J.R., PlascenciaVilla, G., Jose-Yacaman, M., Gardea-Torresdey, J.L., 2012. Comparative toxicity assessment of CeO₂ and ZnO nanoparticles towards *Sinorhizobium meliloti*, a symbiotic alfalfa associated bacterium: use of advanced microscopic and spectroscopic techniques. *J. Hazard. Mater.* 241–242, 379–386.

- Bang, J.H., Suslick, K.S., 2010. Applications of ultrasound to the synthesis of nanostructured materials. *Adv. Mater.* 22, 1039.
- Bao, Y., An, W., Turner, C.W., Krishnan, K.M., 2010. The critical role of surfactants in the growth of cobalt nanoparticles. *Langmuir* 26, 478–483.
- Bao, H., Zhang, Z., Hua, Q., Huang, W., 2014. Compositions, structures, and catalytic activities of $\text{CeO}_2@\text{Cu}_2\text{O}$ nanocomposites prepared by the template-assisted method. *Langmuir* 30, 6427–6436.
- Borkow, G., Gabbay, J., 2009. Copper an ancient remedy returning to fight microbial, fungal and viral infections. *Curr. Chem. Biol.* 3, 272–278.
- Bradley, D.C., Mehrotra, R.C., Rothwell, I.P., Singh, A., 2001. Alkoxo and Aryloxo Derivatives of Metals. Academic Press, London.
- Brust, M., Walker, M., Bethell, D., Schiffrin, D.J., Whyman, R., 1994. Synthesis of thiol-derivatised gold nanoparticles in a two-phase liquid-liquid system. *J. Chem. Soc. Chem. Commun.* 7, 801.
- Carroll, K.J., Reveles, J.U., Shultz, M.D., Khanna, S.N., Carpenter, E.E., 2011. Preparation of elemental Cu and Ni nanoparticles by the polyol method: an experimental and theoretical approach. *J. Phys. Chem. C* 115, 2656–2664.
- Castro, L., Blazquez, Munoz, M.L., Gonzalez, J.A.F., Garcia-Balboa, C., Ballester, A., 2011. Biosynthesis of gold nanowires using sugar beet pulp. *Process Biochem.* 46, 1076–1082.
- Chen, S., Carroll, D.L., 2002. Synthesis and characterization of truncated triangular silver nanoplates. *Nano Lett.* 2, 1003–1007.
- Chen, Y., Peng, D.L., Lin, D., Luo, X., 2007. Preparation and magnetic properties of nickel nanoparticles via the thermal decomposition of nickel organometallic precursor in alkylamines. *Nanotechnology* 18, 505703.
- Conde, J., Doria, G., Baptista, P., 2011. Noble metal nanoparticles applications in cancer. *J. Drug Del.* 2012, 1–12.
- Cormode, D.P., Skajaa, T., van Schooneveld, M.M., Koole, R., Jarzyna, P., Lobatto, M.E., Calcagno, C., Barazza, A., Gordon, R.E., Zanzonico, P., Fisher, E.A., Fayad, Z.A., Mulder, W.J., 2008. Nanocrystal core high-density lipoproteins: a multimodality contrast agent platform. *Nano Lett.* 8, 3715–3723.
- Corriu, R.J.P., Leclercq, D., 1996. Recent developments of molecular chemistry for sol-gel processes. *Angew. Chem. Int. Ed.* 35, 1420–1436.
- Cushing, B.L., Kolesnichenko, V.L., O'Connor, C.J., 2004. Recent advances in the liquid-phase syntheses of inorganic nanoparticles. *Chem. Rev.* 104, 3893–3946.
- Deng, Z., Chen, M., Gu, G., Wu, L., 2008. A facile method to fabricate ZnO hollow spheres and their photocatalytic property. *J. Phys. Chem. B* 112, 16–22.
- Diab, M., Moshofsky, B., Plante, I.J.L., Mokari, T., 2011. A facile one-step approach for the synthesis and assembly of copper and copper-oxide nanocrystals. *J. Mater. Chem.* 21, 11626–11630.
- Dickson, R.M., Lyon, L.A., 2000. Unidirectional plasmon propagation in metallic nanowires. *J. Phys. Chem. B* 104, 6095–6098.
- Dobson, J., 2006. Magnetic nanoparticles for drug delivery. *Drug Dev. Res.* 67, 55–60.
- Edmundson, M., Thanh, N.T., Song, B., 2003. Nanoparticles based stem cell tracking in regenerative medicine. *Theranostics* 3, 573–582.
- El Badawy, A.M., Silva, R.G., Morris, B., Scheckel, K.G., Suidan, M.T., Tolaymat, T.M., 2011. Surface charge-dependent toxicity of silver nanoparticles. *Environ. Sci. Technol.* 1, 283–287.
- Feng, X., Ma, H., Huang, S., Pan, W., Zhang, X., Tian, F., Gao, C., Cheng, Y., Luo, J., 2006. Aqueous-organic phase-transfer of highly stable gold, silver, and platinum nanoparticles and new route for fabrication of gold nanofilms at the oil/water interface and on solid supports. *J. Phys. Chem. B* 110, 12311–12317.
- Fleischmann, M., Hendra, P.J., McQuillan, A.J., 1974. Raman spectra of pyridine adsorbed at a silver electrode. *Chem. Phys. Lett.* 26, 163–166.
- Fresta, M., Wehrli, E., Puglisi, G., 1995. Enhanced therapeutic effect of cytidine-5¢-diphosphate choline when associated with G (M1) containing small liposomes as demonstrated in a rat ischemia model. *Pharm. Res.* 12, 1769–1774.

- Galper, M.W., Saung, M.T., Fuster, V., Roessl, E., Thran, A., Proksa, R., Fayad, Z.A., Cormode, D.P., 2012. Effect of computed tomography scanning parameters on gold nanoparticle and iodine contrast. *Invest. Radiol.* 47, 475–481.
- Gerbec, J.A., Magana, D., Washington, A., Strouse, G.F., 2005. Microwave enhanced reaction rates for nanoparticle synthesis. *J. Am. Chem. Soc.* 127, 15791–15800.
- Grisaru, H., Palchik, O., Gedanken, A., Palchik, V., Slifkin, M.A., Weiss, A.M., 2003. Microwave-assisted polyol synthesis of CuInTe₂ and CuInSe₂ nanoparticles. *Inorg. Chem.* 42, 7148–7155.
- Gunawan, C., Teoh, W.Y., Marquis, C.P., Amal, R., 2011. Cytotoxic origin of copper (II) oxide nanoparticles: comparative studies with micron-sized particles, leachate, and metal salts. *ACS Nano* 5, 7214–7225.
- Gundiah, G., Mukhopadhyay, S., Tumkurkar, U.G., Govindaraj, A., Maitra, U., Rao, C.N.R., 2003. Hydrogel route to nanotubes of metal oxides and sulfates. *J. Mater. Chem.* 13, 2118–2122.
- Hakuta, Y., Ura, H., Hayashi, H., Arai, K., 2005. Continuous production of BaTiO₃ nanoparticles by hydrothermal synthesis. *Ind. Eng. Chem. Res.* 44, 840–846.
- Hu, X., Gong, J., Zhang, L.Z., Yu, J.C., 2008. Continuous size tuning of monodisperse ZnO colloidal nanocrystal clusters by a microwave polyol process and their application for humidity sensing. *Adv. Mater.* 20, 4845–4850.
- Hu, X.L., Yu, J.C., 2008. Continuous aspect-ratio tuning and fine shape control of monodisperse alpha-Fe₂O₃ nanocrystals by a programmed microwave-hydrothermal method. *Adv. Funct. Mater.* 18, 880–887.
- Huang, X., El-Sayed, I.H., Qian, W., El-Sayed, M.A., 2006b. Cancer cell imaging and photothermal therapy in the nearinfrared region by using gold nanorods. *J. Am. Chem. Soc.* 128, 2115–2120.
- Huang, X., Jain, P.K., El-Sayed, I.H., El-Sayed, M.A., 2006a. Determination of the minimum temperature required for selective photothermal destruction of cancer cells with the use of immunotargeted gold nanoparticles. *Photobioch. Photobiop.* 82, 412–417.
- Jain, N., Bhargava, A., Majumdar, S., Panwar, J., 2011. Extracellular biosynthesis and characterization of silver nanoparticles using *Aspergillus flavus*NJP08: a mechanism prospective. *Nanoscale* 3, 635–641.
- Joo, J., Kwon, S.G., Yu, J.H., Hyeon, T., 2005. Synthesis of ZnO nanocrystals with cone, hexagonal cone, and rod shapes via nonhydrolytic ester elimination sol-gel reactions. *Adv. Mater.* 17, 1873–1877.
- Kang, Y., Murray, C.B., 2010. Synthesis and electrocatalytic properties of cubic Mn-Pt nanocrystals. *J. Am. Chem. Soc.* 132, 7568–7569.
- Kashchiev, D., van Rosmalen, G.M., 2003. Review-Nucleation in solutions revisited. *Cryst. Res. Technol.* 38, 555.
- Kim, D., Park, J., An, K., Yang, N.K., Park, J.G., Hyeon, T., 2007. Synthesis of hollow iron nanoframes. *J. Am. Chem. Soc.* 129, 5812–5813.
- Kim, K.S., Demberelnyamba, D., Lee, H., 2004. Size-selective synthesis of gold and platinum nanoparticles using novel thiol functionalized ionic liquids. *Langmuir* 20, 556–560.
- Kim, S.W., Park, J., Jang, Y., Chung, Y., Hwang, S., Hyeon, T., Kim, Y.W., 2003. Synthesis of Monodisperse Palladium Nanoparticles. *Nano Lett.* 3, 1289–1291.
- Kura, H., Takahashi, M., Ogawa, T., 2010. Synthesis of monodisperse iron nanoparticles with a high saturation magnetization using an Fe(CO)x-oleylamine reacted precursor. *J. Phys. Chem. C* 114, 5835–5838.
- Kwon, S.G., Hyeon, T., 2008. Colloidal chemical synthesis and formation kinetics of uniformly sized nanocrystals of metals, oxides, and chalcogenides. *Acc. Chem. Res.* 41, 1696–1709.
- Lemire, J.A., Harrison, J.J., Raymond, J., 2013. Antimicrobial activity of metals: mechanisms, molecular targets and applications. *Nat. Rev. Microbiol.* 11, 371–384.
- Li, C., Sun, L., Sun, Y., Teranishi, T., 2013. One-pot controllable synthesis of Au@Ag heterogeneous nanorods with highly tunable plasmonic absorption. *Chem. Mater.* 25, 2580–2590.
- Li, S., Shen, Y., Xie, A., Yu, X., Qiu, L., Zhang, L., Zhang, Q., 2007. Green synthesis of silver nanoparticles using *Capsicum annuum* L. extract. *Green Chem.* 9, 852–858.
- Li, X.L., Peng, Q., Yi, J.X., Wang, X., Li, Y., 2006. Near monodisperse TiO₂ nanoparticles and nanorods. *Chem. Eur. J.* 12, 2383–2391.
- Liu, Z., Fan, T., Zhang, W., Zhang, D., 2005. The synthesis of hierarchical porous iron oxide with wood templates. *Micropor. Mesopor. Mater.* 85, 82–88.

- Luef, B., Fakra, S.C., Csencsits, R., Wrighton, K.C., Williams, K.H., Wilkins, M.J., Downing, K.H., Long, P.E., Comolli, L.R., Banfield, J.F., 2013. Iron-reducing bacteria accumulate ferric oxyhydroxide nanoparticle aggregates that may support planktonic growth. *ISME J.* 7, 338–350.
- Luo, X., Chen, Y., Yue, G.-H., Peng, D.-L., Luo, X., 2009. Preparation of hexagonal close-packed nickel nanoparticles via a thermal decomposition approach using nickel acetate tetrahydrate as a precursor. *J. Alloy Compd.* 476, 864–868.
- Maeda, H., Wu, J., Sawa, T., Matsumura, Y., Hori, K., 2000. Tumor vascular permeability and the EPR effect in macromolecular therapeutics: a review. *J. Control. Release* 65, 271–284.
- Mallikarjuna, N.N., Varma, R.S., 2007. Microwave-assisted shape-controlled bulk synthesis of noble nanocrystals and their catalytic properties. *Cryst. Growth Des.* 7, 686–690.
- Moghimi, S.M., Patel, H.M., 1998. Serum-mediated recognition of liposomes by phagocytic cells of the reticuloendothelial system—the concept of tissue specificity. *Adv. Drug Deliv. Rev.* 32, 45–60.
- Mohamed, M.B., AbouZeid, K.M., Abdelsayed, V., Aljarash, A.A., Samy El-Shall, M., 2010. Growth mechanism of anisotropic gold nanocrystals via microwave synthesis: formation of dioleamide by gold nanocatalysis. *ACS Nano* 4, 2766–2772.
- Morones, J.R., Elechiguerra, J.L., Camacho, A., Holt, K., Kouri, J.B., Ramirez, J.T., Yacaman, M.J., 2005. The bactericidal effect of silver nanoparticles. *Nanotechnology* 16, 2346–2353.
- Nath, D., Banerjee, P., 2013. Green nanotechnology—a new hope for medical biology. *Environ. Toxicol. Pharmacol.* 36, 997–1014.
- Nichols, J.W., Bae, Y.H., 2012. Odyssey of a cancer nanoparticle from injection site to site of action. *Nano Today* 7, 606–618.
- Niederberger, M., 2007. Nonaqueous sol-gel routes to metal oxide nanoparticles. *Acc. Chem. Res.* 40, 793–800.
- Njagi, E.C., Huang, H., Stafford, L., Genuino, H., Galindo, H.M., Collins, J.B., Hoag, G.E., Steven, L.S., 2011. Biosynthesis of iron and silver nanoparticles at room temperature using aqueous sorghum bran extracts. *Langmuir* 27, 264–271.
- Okada, T., Sasaki, F., Kamiyama, T., Nakagawa, T., Nakanishi, K., Kobayashi, R., 2005. Focal nodular hyperplasia of the liver: usefulness of super paramagnetic iron oxide-enhanced magnetic resonance imaging. *J. Pediatr. Surg.* 40, E21–E25.
- Okitsu, K., Sharyo, K., Nishimura, R., 2009. One-pot synthesis of gold nanorods by ultrasonic irradiation: the effect of pH on the shape of the gold nanorods and nanoparticles. *Langmuir* 25, 7786–7790.
- Pal, S., Tak, Y.K., Song, J.M., 2007. Does the antibacterial activity of silver nanoparticles depend on the shape of the nanoparticle? A study of the Gram-negative bacterium *Escherichia coli*. *Appl. Environ. Microbiol.* 73, 1712–1720.
- Patete, J.M., Peng, X., Koenigsmann, C., Xu, Y., Karn, B., Wong, S.S., 2011. Viable methodologies for the synthesis of high-quality nanostructures. *Green Chem.* 13, 482–519.
- Payne, E.K., Shuford, K.L., Park, S., Schatz, G.C., Mirkin, C.A., 2006. Multipole plasmon resonances in gold nanorods. *J. Phys. Chem. B* 110, 2150–2154.
- Prakash, B., 1997. Use of metals in Ayurvedic medicine. *Indian J. History Sci.* 32, 1–28.
- Prasad, B.L.V., Arumugam, S.K., Bala, T., Sastry, M., 2005. Solvent-adaptable silver nanoparticles. *Langmuir* 21, 822–826.
- Qian, X., Shen, S., Liu, T., Cheng, L., Liu, Z., 2015. Two-dimensional TiS₂ nanosheets for in vivo photoacoustic imaging and photothermal cancer therapy. *Nanoscale* 7, 6380–6387.
- Rabenau, A., 1985. The role of hydrothermal synthesis in preparative chemistry. *Angew. Chem. Int. Ed. Engl.* 24, 1026–1040.
- Rao, C.N.R., Kalyanikutty, K.P., 2008. The liquid–liquid interface as a medium to generate nanocrystalline films of inorganic materials. *Acc. Chem. Res.* 41, 489–499.
- Rao, C.N.R., Kulkarni, G.U., John Thomas, P., Agrawal, V.V., Saravanan, P., 2003. Films of metal nanocrystals formed at aqueous-organic interfaces. *J. Phys. Chem. B* 107, 7391–7395.

- Rao, C.N.R., Ramakrishna Matte, H.S.S., Voggu, R., Govindaraj, A., 2012. Recent progress in the synthesis of inorganic nanoparticles. *Dalton Trans.* 41, 5089.
- Reddy, B.M., Reddy, G.K., Ganesh, I., Ferreira, J.M.F., 2009a. Microwave-assisted synthesis and structural characterization of nanosized $\text{Ce}_{0.5}\text{Zr}_{0.5}\text{O}_3$ for CO oxidation. *Catal. Lett.* 130, 227–234.
- Reddy, B.M., Reddy, G.K., Ganesh, I., Ferreira, J.M.F., 2009b. Single step synthesis of nanosized $\text{CeO}_2\text{-M}_x\text{O}_y$ mixed oxides ($\text{M}_x\text{O}_y=\text{SiO}_2$, TiO_2 , ZrO_2 , and Al_2O_3) by microwave induced solution combustion synthesis: characterization and CO oxidation. *J. Mater. Sci.* 44, 2743–2751.
- Reddy, B.M., Reddy, G.K., Rao, K.N., Ganesh, I., Ferreira, J.M.F., 2009c. Characterization and photocatalytic activity of $\text{TiO}_2\text{-M}_x\text{O}_y$ ($\text{M}_x\text{O}_y=\text{SiO}_2$, Al_2O_3 , and ZrO_2) mixed oxides synthesized by microwave-induced solution combustion technique. *J. Mater. Sci.* 44, 4874–4882.
- Reddy, B.M., Reddy, G.K., Katta, L., 2010. Structural characterization and dehydration activity of $\text{CeO}_2\text{-SiO}_2$ and $\text{CeO}_2\text{-ZrO}_2$ mixed oxides prepared by a rapid microwave-assisted combustion synthesis method. *J. Mol. Catalysis A Chem.* 319, 52–57.
- Richter, K., Birkner, A., Mudring, A.V., 2010. Stabilizer-free metal nanoparticles and metal-metal oxide nanocomposites with long-term stability prepared by physical vapor deposition into ionic liquids. *Angew. Chem. Int. Ed.* 49, 2431–2435.
- Rycenga, M., Wang, Z., Gordon, E., Cobley, C.M., Schwartz, A.G., Lo, C.S., Xia, Y., 2009. Probing the photothermal effect of gold-based nanocages with surface-enhanced Raman scattering (SERS). *Angew. Chem. Int. Ed.* 48, 9924–9927.
- Samia, A.C.S., Schlueter, J.A., Jiang, J.S., Bader, S.D., Qin, C.J., Lin, X.M., 2006. Effect of ligand-metal interactions on the growth of transition-metal and alloy nanoparticles. *Chem. Mater.* 18, 5203–5212.
- Sathishkumar, M., Sneha, K., Kwak, I.S., Mao, J., Tripathy, S.J., Yun, Y.-S., 2009. Phyto-crystallization of palladium through reduction process using *Cinnamom zeylanicum* bark extract. *J. Hazard. Mater.* 171, 400–404.
- Sathishkumar, B.C., Govindaraj, A., Nath, M., Rao, C.N.R., 2000. Synthesis of metal oxide nanorods using carbon nanotubes as templates. *J. Mater. Chem.* 10, 2115–2119.
- Seo, J.-W., Jun, Y.-W., Ko, S.J., Cheon, J., 2005. In situ one-pot synthesis of 1-dimensional transition metal oxide nanocrystals. *J. Phys. Chem. B* 109, 5389–5391.
- Shi, W., Song, S., Zhang, H., 2013. Hydrothermal synthetic strategies of inorganic semiconducting nanostructures. *Chem. Soc. Rev.* 42, 5714–5743.
- Shiv Shankar, S., Ahmad, A., Pasricha, R., Sastry, M., 2003. Bioreduction of chloroaurate ions by geranium leaves and its endophytic fungus yields gold nanoparticles of different shapes. *J. Mater. Chem.* 13, 1822–1826.
- Skrabalak, S.E., Chen, J., Sun, Y., Lu, X., Au, L., Cobley, C.M., Xia, Y., 2008. Gold nanocages: synthesis, properties, and applications. *Acc. Chem. Res.* 41, 1587–1595.
- Song, Q., Zhang, Z.J., 2004. Shape control and associated magnetic properties of spinel cobalt ferrite nanocrystals. *J. Am. Chem. Soc.* 126, 6164–6168.
- Stoimenov, P.K., Klinger, R.L., Marchin, G.L., Klabunde, K.J., 2002. Metal oxide nanoparticles as bactericidal agents. *Langmuir* 18, 6679–6686.
- Suslick, K.S., 1990. Sonochemistry. *Science* 247, 1439.
- Suslick, K.S., Price, G.J., 1999. Applications of ultrasound to materials chemistry. *Annu. Rev. Mater. Sci.* 29, 295.
- Taton, T.A., Mirkin, C.A., Letsinger, R.L., 2000. Scanometric DNA array detection with nanoparticle probes. *Science* 289, 1757–1760.
- Tsuji, M., Hashimoto, M., Nishizawa, Y., Kubokawa, M., Tsuji, T., 2005. Microwave-assisted synthesis of metallic nanostructures in solution. *Chem. Eur. J.* 11, 440–452.
- Turova, N.Y., Turevskaya, E.P., 2002. The Chemistry of Metal Alkoxides. Kluwer Academic Publishers, Boston.
- Van, T.-K., Cha, H.G., Nguyen, C.K., Kim, S.-W., Jung, M.-H., Kang, Y.S., 2012. Nanocrystals of hematite with unconventional shape-truncated hexagonal bipyramid and its optical and magnetic properties. *Cryst. Growth Des.* 12, 862–868.

- von Maltzahn, G., Park, J.-H., Agrawal, A., 2009. Computationally guided photothermal tumor therapy using long-circulating gold nanorod antennas. *Cancer Res.* 69, 3892–3900.
- Wang, H., Brandl, D.W., Nordlander, P., Halas, N.J., 2007. Plasmonic nanostructures: artificial molecules. *Acc. Chem. Res.* 40, 53–62.
- Wang, Y., Zheng, Y., Huang, C.Z., Xia, Y., 2013. Synthesis of Ag nanocubes 18–32 nm in edge length: the effects of polyol on reduction kinetics, size control, and reproducibility. *J. Am. Chem. Soc.* 135, 1941–1951.
- Wu, M., Lin, G., Chen, D., Wang, G., He, D., Feng, S., Xu, R., 2002. Sol-hydrothermal synthesis and hydrothermally structural evolution of nanocrystal titanium dioxide. *Chem. Mater.* 14, 1974–1980.
- Xiu, Z.M., Zhang, Q.B., Puppala, H.L., Colvin, V.L., Alvarez, P.J., 2012. Negligible particle-specific antibacterial activity of silver nanoparticles. *Nano Lett.* 12, 4271–4275.
- Xu, H., Zeiger, B.W., Suslick, K.S., 2013. Sonochemical synthesis of nanomaterials. *Chem. Soc. Rev.* 42, 2555–2567.
- Yan, L., Yu, R., Chen, J., Xing, X., 2008. Template-free hydrothermal synthesis of CeO₂ nano-octahedrons and nanorods: investigation of the morphology evolution. *Cryst. Growth Des.* 8, 1474–1477.
- Yang, J., Lee, J.Y., Ying, J.Y., 2011. Phase transfer and its applications in nanotechnology. *Chem. Soc. Rev.* 40, 1672–1696.
- Yang, J., Sargent, E., Kelley, S., Ying, J.Y., 2009. A general phase-transfer protocol for metal ions and its application in nanocrystal synthesis. *Nat. Mater.* 8, 683.
- Yang, Z., Han, D., Ma, D., Liang, H., Liu, L., Yang, Y., 2010. Fabrication of monodisperse CeO₂ hollow spheres assembled by nano-octahedra. *Cryst. Growth Des.* 10, 291–295.
- Zeng, H., Rice, P.M., Wang, S.X., Sun, S.H., 2004. Shape-controlled synthesis and shape-induced texture of MnFe₂O₄ nanoparticles. *J. Am. Chem. Soc.* 126, 11458–11459.
- Zhang, L.-S., Jiang, L.-Y., Chen, C.-Q., Li, W., Song, W.-G., Guo, Y.-G., 2010a. Programmed fabrication of metal oxides nanostructures using dual templates to spatially disperse metal oxide nanocrystals. *Chem. Mater.* 22, 414–441.
- Zhang, Q., Liu, F., Nguyen, K.T., Ma, X., Wang, X., Xing, B., Zhao, Y., 2012. Multifunctional mesoporous silica nanoparticles for cancer-targeted and controlled drug delivery. *Adv. Funct. Mater.* 22, 5144–5156.
- Zhang, Y., Yu, J., Birch, D.J., Chen, Y., 2010b. Gold nanorods for fluorescence lifetime imaging in biology. *J. Biomed. Opt.* 15, 020504.
- Zheng, U., Liu, S., Chen, X., Cheng, J., Si, C., Pan, Z., Marcelli, A., Chu, W., Wu, Z., 2003. Synthesis and characterization of cu-pt bimetallic nanoparticles. *J. Phys.* 430, 012037.
- Zili, W., Li, M., Overbury, S.H., 2012. On the structure dependence of CO oxidation over CeO₂ nanocrystals with well-defined surface planes. *J. Catalysis* 285, 61–73.
- Zitoun, D., Pinna, N., Frolet, N., Belin, C., 2005. Single crystal manganese oxide multipods by oriented attachment. *J. Am. Chem. Soc.* 127, 15034–15035.